Fuse State Estimation and Sequence Control for Enhancing Current Limiting Performance in Hybrid DC Circuit Breakers
ヒューズ半導体ハイブリッド直流遮断器のヒューズ状態推定とシーケンス制御による限流性能向上に関する研究

by

37-236555
Songah Shin
シン ソングア

Master Thesis
修士論文

Submitted for the Degree of
Master of Engineering
at
Department of Electrical Engineering and Information Systems
Graduate School of Engineering
The University of Tokyo
January 23rd, 2025

Thesis Supervisor: Wataru Ohnishi　大西 亘
Professor of Electrical Engineering and Information Systems

ABSTRACT

The growing need for the development and integration of DC systems has led advancements in direct current (DC) circuit breakers (CBs). Among the three main types of DC CBs, hybrid DC CBs are now widely used solution in DC transmission and distribution systems. However, high cost and large size challenges remain. To address these issues, our team developed a hybrid DC CB that combines a current-limiting fuse and a semiconductor device.

In this configuration, the rated current flows through the fuse branch. When a fault current occurs, the current-limiting fuse reduces the current, and the current path is switched to the IGBT branch once the current is sufficiently reduced. If commutation occurs too quickly, the IGBT may explode. Conversely, if the commutation is delayed, the fuse may explode. Thus, determining the optimal timing to change the current path based on the fuse's status is critical for completing the interruption process in the DC CB. Our team proposed a commutation method that uses real-time fuse current data to solve this challenge. However, this method was validated only once under explosive conditions, utilizing a specific type of fuse.

In this thesis, the robustness of the previously proposed current-based fuse state estimation is evaluated using two types of fuses, a ceramic fuse and a glass fuse, under various electrical conditions: 1.7 kV and 10 kA, 0.95 kV and 10 kA, and 0.4 kV and 0.5 kA.

Based on these experiments, several limitations were identified:

- Gap between physical phenomena and current data
- Delay in sending the signal to the IGBT
- Premature commutation error
- Commutation operation when fuse-only interruption is feasible

To overcome these limitations, a current-voltage-based method for commutation is proposed. Specifically, an energy criterion is applied to determine the commutation. The minimum energy threshold was simulated using the arcing current model with a single $\frac{1}{R_{\text{arc}}C_{\text{arc}}}$ value derived from previous experimental data. The maximum energy threshold was simulated based on Joule's law, with energy calculated using data collected up to the point of resurgence. Using this simulation, the energy criterion was set at 9 kJ and validated under experimental conditions of 1.6 kV and 10 kA. The results showed that energy was accurately calculated in real-time and that commutation was successfully initiated.

This approach addresses the limitations of the current-based method. First, since the commutation method is based on energy, it provides a clearer understanding of the physical state of the fuse and the

internal phenomena. Additionally, this method eliminates delays by not relying on the RLS algorithm to determine the commutation time. The premature commutation error is resolved by the minimum energy threshold, which prevents commutation from occurring until the accumulated energy exceeds the threshold. This threshold also ensures that commutation does not occur when the fuse can independently interrupt the fault current.

Acknowledgements

The two years I spent at the Koseki-Ohnishi Laboratory were very special and meaningful. I want to thank everyone who supported me during this journey and helped me complete my research.

I am deeply grateful to Prof. Ohnishi for his guidance and insight, which were the key to finish this study. I admire how he inspires students with his knowledge and creates an environment of curiosity and learning. This had a great impact on my research life for two years in the master's course. I also want to thank Prof. Koseki for his support, advice, and encouragement, which motivated me and helped me achieve this academic goal.

I would also like to express my sincere appreciation to Mr. Takada for his technical advice and encouragement during the many challenges I faced in the experiments. His support helped me develop the ability to use various experimental equipment and design experiments. Furthermore, I am very grateful to Mrs. Matsuzaki for her kind assistance, which made me gradually get used to the working procedures in a new environment.

I thank the members of the DCCB team. Sasaki has always shown me how to conduct research in the best way. His clear explanations about the research background and the role of each component helped me understand both the large concept and the details of each experiment. Nakano's enthusiasm also inspired and motivated me to focus on my own research.

I want to thank Sakai and Ueno for leading the weekly lab meetings and organizing the lab activities. Additionally, I also enjoyed working with Nagai and MB during these two years and wish them the best as they continue their research as Ph.D. students.

Finally, I am very grateful to my international student friends Meng, Yang, Sun, and Gao, who shared their experiences and gave me advice and encouragement about life in Japan. I also cherish the joyful times I spent with Edisa, Li, and Chang. Although our time together was short, the memories we shared in 2024 made my time here even more special.

Contents

List of Figures

List of Tables

Chapter 1

Introduction

The growing need for the development and integration of DC systems that include electrical vehicles, industrial power systems, and renewable energy sources as shown Fig.1.1 has led to the further development of direct current (DC) circuit breakers (CB) [2]. Because DC CB does not achieve zero crossing naturally, it has to create an artificial zero point in the current. The fundamental functions of DC CBs are: 1) the control of the opening and closing of circuits, and 2) the isolation of fault current DC lines in case of faults [3].

(a) Electrical vehicle

(b) Industrial power systems

(c) Renewable energy sources

Figure 1.1: DC systems where DC CB is required

Considering the required functions, three main types of DC circuit breakers have been developed: mechanical DC CB, solid-state DC CB, and hybrid DC CB [4]. A detailed comparison of the three types of DC CB is presented in Table.1.1. A mechanical DC CB is based on a conventional AC CB but includes a parallel resonant circuit. The LC circuit interrupts by creating an artificial zero current point [5]. This breaker is usually applied for medium voltage and power levels [6]. The principle of operation of solid-state DC CBs is based on the interruption by power electronic devices [7]. Conventional mechanical CBs are cheap and their power loss is low, but they have some issues with a long shut-off time, oversize, and easy to cause an arc

[7, 8, 9]. On the other hand, traditional solid-state DC CBs are much faster than mechanical DC CBs without requiring a current zero crossing, but have the disadvantages of power loss and higher cost [7]. Because of these aspects, a new configuration is usually based on the hybrid model.

Table. 1.1: Comparison between Mechanical, Solid-State, and Hybrid DC CBs

Criteria	Mechanical DCCB	Solid-State DCCB	Hybrid DCCB
Break Time [2, 10]	5~10 ms	~100 μs	2~5 ms
Break Current [2, 6, 10]	~4 kA	~6 kA	16~25 kA
On-State Losses [2]	Negligible	~100 mΩ	<5 mΩ
Cost (6 kV) [11]	5.8 k$	6.4 k$	8.7 k$
Size [12]	Large	Compact	Large

1.1 Literature review of DC circuit breakers

Hybrid DC CBs are the mainstream solution used in DC transmission and distribution systems nowadays. After ABB [13] proposed a hybrid HVDC breaker, which has negligible conduction losses while preserving ultra-fast current interruption capability, several attempts have been made for new configurations of hybrid DC CBs.

Ou *et al.* [14] increased the contact threshold current using a cuboid shape with a join of copper and carbon. Hassanpoor *et al.* [15] presented several modified snubber designs, which are appropriate for a bidirectional load commutation switch to run the fast interruption action. Koyama *et al.* [16] invented a multiline hybrid DC CB model, which can share semiconductor breakers. Thus, it is possible to reduce the breaker components. In [17], a thyristor alternated the semiconductor devices to design a cost-efficient model. Sen *et al.* [12] used two switches together with two diodes to effectively break the fault current with minimal arc and reduce the voltage stress.

However, the switching speed, which is one of the important factors in DC CB, still strongly depends on the mechanical switch in the system. In addition, a fault current limiter is necessary to safely interrupt the current when the fault currents exceed 10 kA. There are three types of fault

current limiters: 1) current-limiting reactors, 2) superconductors, and 3) current-limiting fuses. The first one has a high cost and its efficiency is low, and the second one is expensive to run the system and has a burning risk. Therefore, considering the cost, efficiency, and complexity, the current-limiting fuse is desirable [1].

1.2 Fuse-semiconductor hybrid DC circuit breakers

Zen *et al.* [1] proposed a hybrid DC CB that limits current, which incorporates a current-limiting fuse and a semiconductor device without mechanical contact. Fig.1.2 shows the proposed DC CB diagram. This configuration enables the DC CB to achieve both high-speed current limiting and highly reliable current interruption through the combined operation of the fuse and semiconductor device. The performance of this system has been demonstrated in a low-voltage system [18], utilizing a fast fuse exchanger to reactivate the DC CB [19].

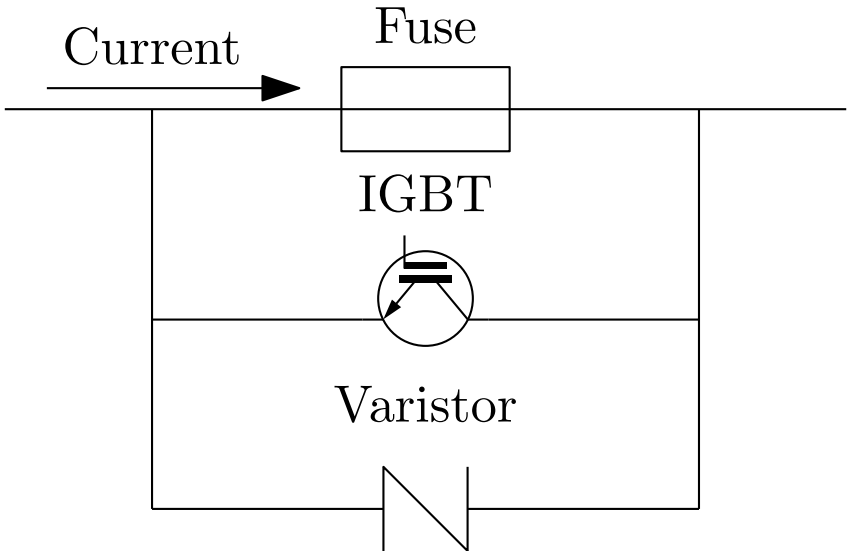

Figure 1.2: Fuse-semiconductor hybrid DC circuit breaker [1]

The operation mechanism is as follows. In nominal status, the rated current passes through the fuse branch. If the fault current is injected into the fuse, the element is melted and evaporated. Then, the energy inside is consumed with heat, and the increasing arc resistance makes an arc voltage higher than the power supply voltage. Therefore, the short-circuit fault current is limited without reaching a peak. When the limited current is reduced enough, the current commutates to the Insulated Gate Bipolar Transistor (IGBT) branch. This branch interrupts the

current after a few milliseconds when the inside of the fuse is insulated by cooling. Finally, the fault current intermission in the hybrid DC CB is completed after the Metal Oxide Varistors (MOVs) absorb the residual energy.

1.3 Research motivation

Initially, the threshold method was utilized to choose the commutation moment in the fuse-semiconductor hybrid DC CB. The threshold was set by the trial-and-error method, which requires prior experiments and measurements. Although this method was well implemented in previous experiments, a more active control method is necessary to safely interact with the variability and diverse waveforms of the fuse current.

Fuses have been developed and widely applied to protect electrical systems from overcurrents or short circuits with the advantage of cost efficiency [20]. However, their operational characteristic is inherently complex to predict and control due to internal multiphysics phenomena [21]. Consequently, determining the optimal timing to switch the current path based on the fuse's status is critical to completing the interruption process in the DC CB. Fig.1.3 shows the dangerous situation that can happen depending on the commutation failure. Fig.1.3a shows the IGBT explosion that can occur when the commutation is premature, whereas Fig.1.3b depicts the fuse explosion situation resulting from delayed commutation.

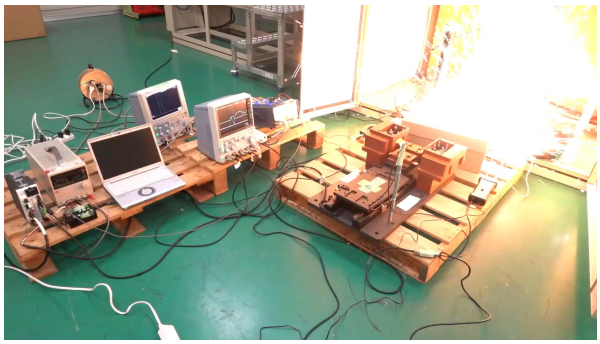

(a) IGBT explosion under early commutation

(b) Fuse explosion under late commutation

Figure 1.3: Risk of explosion due to improper commutation

To solve this risk, Liu *et al.* [22] proposed the commutation method using the data of the fuse current in real-time. This approach presented the fuse state estimation based on the current data. However, fuse state estimation using only current data is limited. In this thesis,

the previously proposed current-based method is demonstrated through comprehensive experiments under various conditions, accompanied by a deeper analysis. In addition, a commutation method is proposed utilizing current and voltage data based on the estimation of the fuse state.

1.4 Outline of the thesis

Fig.1.4 represents the outline of the thesis.

In Chapter 1, the foundational background of the hybrid DC CB is discussed, including its importance and the challenges associated with its development. The concept of integrating fuses and semiconductors in hybrid DC CBs is introduced, as previously developed by our team. Furthermore, the necessity of this commutation-focused research for this fuse-semiconductor hybrid DC CB is highlighted. The chapter concludes with an overview of the thesis structure, outlining the key objectives and the approach to achieving them.

Chapter 2 focuses on the previously proposed current-based commutation method, providing a comprehensive explanation of its operating principles and its application in DC CB systems. Experimental validations are conducted to test the method's robustness and accuracy across a diverse range of conditions. The experimental results form the basis for a detailed analysis of the method to assess its strengths and limitations. This chapter establishes the foundation for understanding the challenges addressed in the subsequent chapters and sets the stage for proposing improvements to the commutation strategy.

Chapter 3 introduces the energy threshold method as a novel commutation strategy that uses both current and voltage data to estimate the real-time state of the fuse. The minimum and maximum energy thresholds are determined through simulations based on the experimental data obtained in Chapter 2. The effectiveness of the proposed method is validated through experiments conducted under high-voltage (1.6 kV) and high-current (10 kA) conditions, demonstrating its reliability and applicability.

Finally, Chapter 4 summarizes the overall content and concludes the thesis by highlighting the key findings and contributions of this research. Recommendations are also provided based on the results of this study.

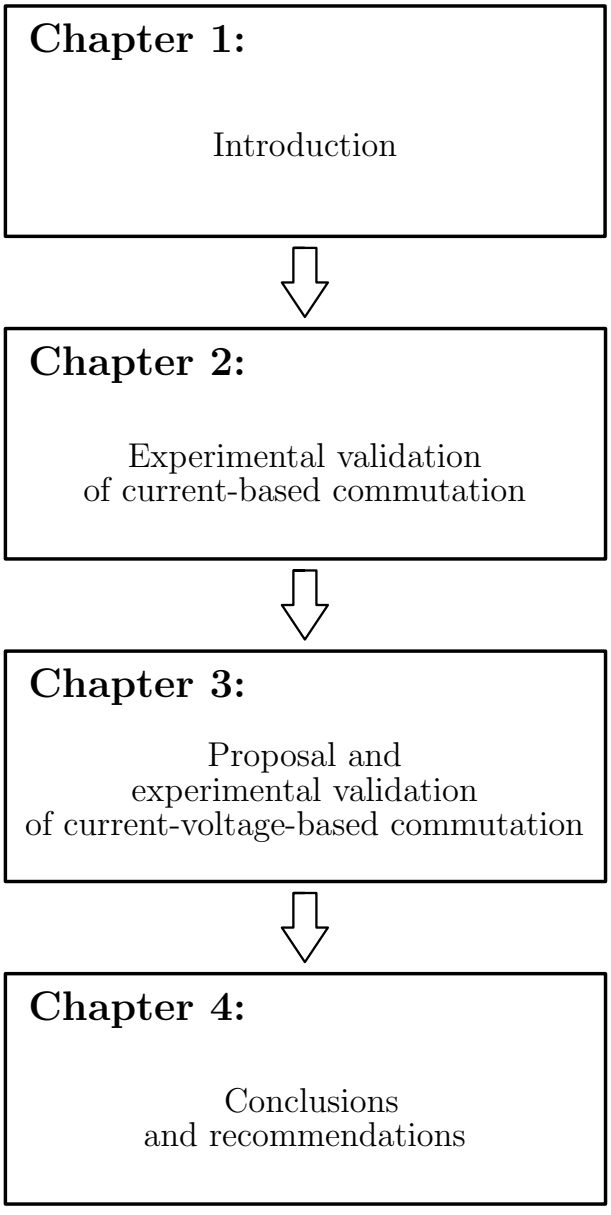

Figure 1.4: Outline of the thesis

Chapter 2

Experimental validation of current-based commutation

2.1 Fuse state estimation using current data

In this section, the previous current-based commutation method [22] will be explained.

2.1.1 Fundamentals of fuses

Initially, it is essential to introduce the fuse blowing process in the successful case of a fault current interruption achieved solely by a fuse. First, the mechanism of a fuse is based on its simple structure, which includes a metal conduction part known as the fuse element [23]. Under nominal conditions, the current passes through the fuse. However, when the current exceeds its rated value, the fuse element heats up because of the increased temperature and eventually melts. As the current continues to flow, it passes through the liquid phase of the fuse element, further increasing its temperature and causing evaporation. The evaporated material ionizes, leading to the formation of an arc between the gaps inside the fuse. This transition is called the pre-arc stage, which occurs just before the arc is fully established. Once the arc forms, it creates a pathway for the current to continue flowing, furthering the fuse element's melting. As the metal continues to melt and diminish, the gap widens and the arc channel weakens. Over time, the weakened arc channel dissipates due to the increased distance, completing the arc process [24]. The fuse state estimation is performed on the basis of the fundamental principles of this fuse blowing process.

Fig.2.1 shows the current and voltage waveforms observed in the fuse during two different

scenarios of the fault current interruption process. Fig.2.1a represents a successful interruption achieved solely by a fuse as described above, while Fig.2.1b illustrates a failed interruption with the current resurge at t = 25 ms. To avoid the later situation, it is necessary to define and analyze the fuse status based on the electrical data.

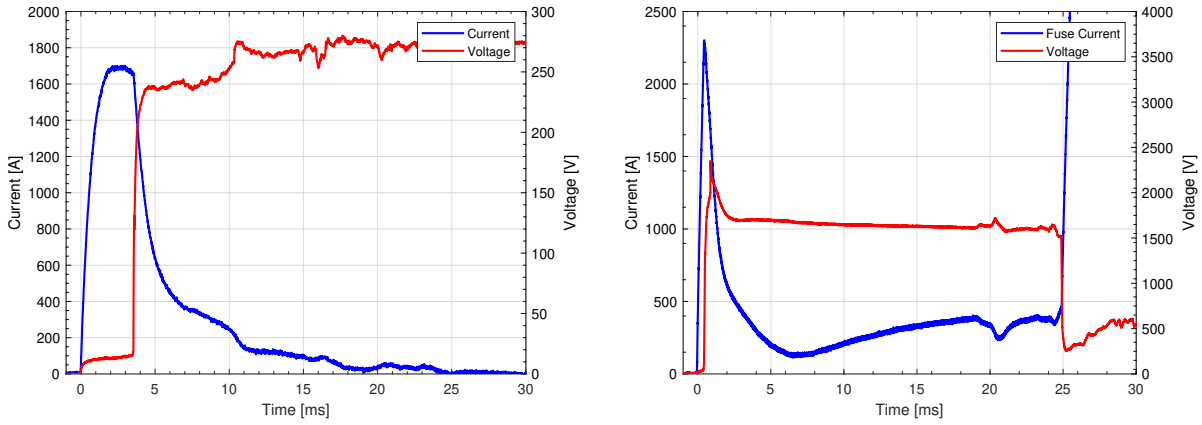

(a) Interruption success

(b) Interruption failure

Figure 2.1: Different fuse current cases

Initially, the fuse current is rapidly limited from the onset of arcing in both cases. In the second phase, the rate of current reduction gradually decreases over time. The difference becomes clear in this phase. In the successful interruption case shown in Fig.2.1a, the current slowly approaches zero. In contrast, in the second case depicted in Fig.2.1b, the current fails to reach zero and eventually starts to increase again, which is represented as the third phase. Therefore, identifying the second and third phases is critical.

To solve this situation, Liu *et al.* [22] proposed the fuse state estimation method using current data on the fuse in real-time to determine the optimal commutation moment. The study concluded that the difference observed in the second phase of the explosion case indicates a reduced current-limiting ability of the fuse. This reduction is attributed to an insufficient medium surrounding the fuse link, which does not absorb the energy from the fault current effectively. This characteristic can serve as a key indicator for switching the current path.

2.1.2 Principle of the current-based commutation

The three phases discussed earlier can be observed in the arcing current. Therefore, modeling and analyzing the arcing current is necessary to understand the fuse's status. Fig.2.1a shows the typical current and voltage waveforms during the successful fuse blowing process. Before the current reaches zero, its gradient varies inconsistently. The literature utilized the resistor-capacitor (RC) discharging circuit model to represent this curve, which follows an exponential decreasing curve. Tanaka *et al.* [25] uses an LCR circuit to model the pre-arcing and arcing currents separately. The RL circuit represents the pre-arcing current, while the RC circuit models the arcing current, and they are connected in parallel through a switch. Li *et al.* [26] describe the current and voltage characteristics during arcing as a combination of the capacitor discharge process and the arc resistance in series. Lee *et al.* [27] presents a voltage model for the arcing period, where the initial voltage rise is due to the capacitor charging process, followed by the discharging process.

The equivalent circuit used to model the fuse current during the arcing period is shown in Fig.2.2 [25, 26]. This circuit is an RC circuit that includes two switches, the fuse switch and the arc switch. It represents the dual functionality of the fuse. Initially, the fuse switch is active before the fuse link melts, which distinguishes the pre-arc stage from the arc stage. When the arc stage begins, the parallel arc switch becomes active, enabling the RC components to represent the arcing current.

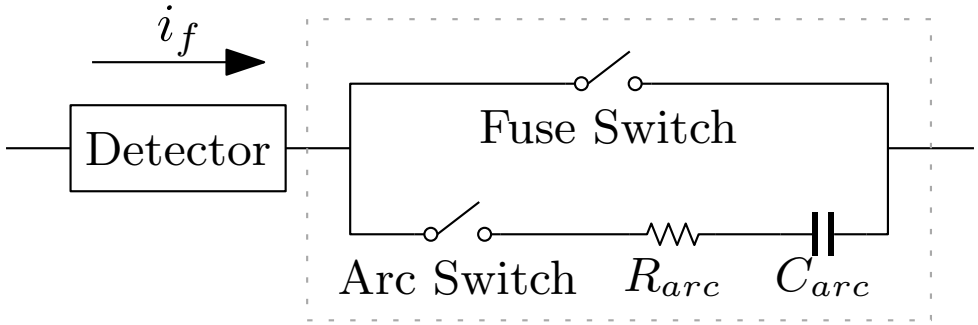

Figure 2.2: RC circuit for modeling the arcing fuse current

The current of the discharging RC circuit can be represented in an exponential function. The following equation can express the mathematical description of the fuse current during the

arcing phase.

$$i(t) = I_0 \, e^{\frac{-t}{R_{arc}C_{arc}}} \tag{2.1}$$

$i(t)$ is the current estimated in real-time flowing through the fuse, and I_0 denotes the maximum current during the arcing period. R_{arc} and C_{arc} determine the shape of the arcing current model.

Li *et al.* [26] utilized the fixed values $R_{arc}C_{arc}$ to represent the specific arc current. These values were derived from the current-voltage characteristic plot obtained in experiments. However, this method is only applicable in successful interruption scenarios. In cases of interruption failure, which results in re-arcing and a resurge of current in the fuse, the fixed $R_{arc}C_{arc}$ values cannot accurately model the behavior. Fig.2.3 shows that the re-arcing current scenario needs varying $R_{arc}C_{arc}$ values to match the actual current data using the arcing circuit model. Two distinct $R_{arc}C_{arc}$ values, 0.93 and 1.79, are used to model different sections of the current data. Consequently, a real-time calculation of dynamic $R_{arc}C_{arc}$ values is essential to efficiently handle multiple cases.

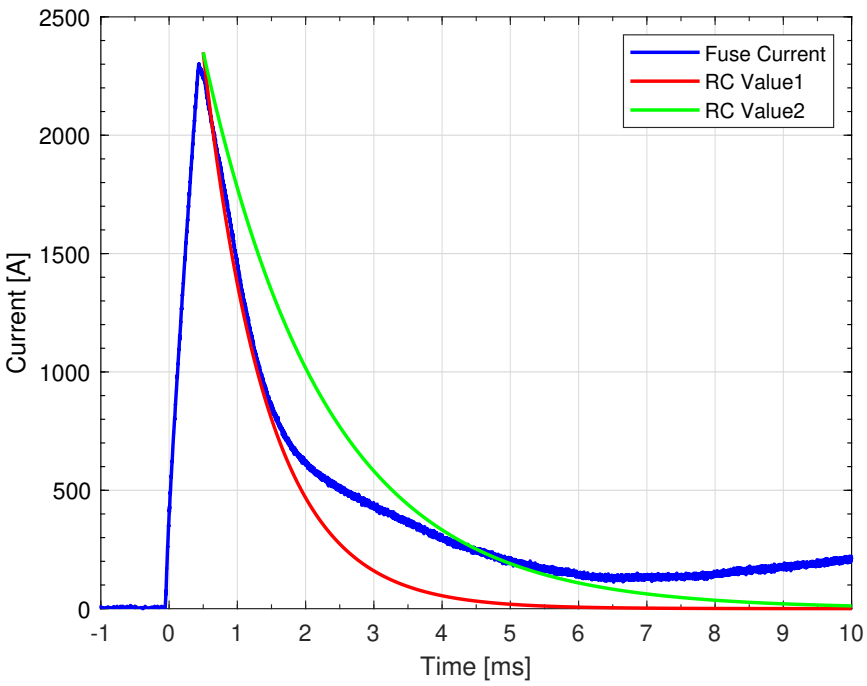

Figure 2.3: Modeled fuse current during the arcing period using two distinct $R_{arc}C_{arc}$ values (0.93, 1.79) in the re-arcing scenario

To update $R_{arc}C_{arc}$ values in real-time to match actual current data, Liu *et al.* [22] adopted the Recursive Least Squares (RLS) algorithm. The RLS algorithm offers the advantages of a fast convergence rate by reducing the computational cost of processing new current data, and the target parameters are computed recursively. This advantage enables the effective identification of $R_{arc}C_{arc}$ values. By continuously updating the parameters, the RLS algorithm ensures a closer match with the actual current during the arcing phase, thereby allowing for a more reliable determination of the current commutation timing.

To apply the RLS algorithm to the commutation process, the RC parameters are integrated as shown in Equation 2.2.

$$\frac{1}{R[n]C[n]} = \beta[n] \tag{2.2}$$

Using Equation 2.2, the estimation of the fuse state in real-time and the calculation of the parameters are performed with the RLS algorithm according to the following equations.

$$\ln(I_0) - \ln(I[n] + \delta) = \beta[n]t[n] \tag{2.3}$$

$$K[n] = \frac{P[n-1] \cdot x[n]}{\lambda + x[n] \cdot P[n-1] \cdot x[n]} \tag{2.4}$$

$$P[n] = \frac{1}{\lambda}(P[n-1] - K[n] \cdot x[n] \cdot P[n-1]) \tag{2.5}$$

$$\beta[n] = \beta[n-1] + K[n] \cdot e[n] \tag{2.6}$$

β is the parameter to be estimated, representing fuse status based on the slope of the decreasing current. The term δ is a small value added to prevent the algorithm from abruptly stopping when the fuse current reaches zero. K denotes the Kalman gain, while P is the error covariance matrix. $x[n]$ indicates time, which increases continuously. λ is the forgetting factor designed to reduce the impact of noise. Finally, e represents the prediction error.

In their research, Liu *et al.* [22] analyzed that when the β parameter reaches its peak, the rate of current decrease is also at its maximum and then starts to decline. This suggests that the current-limiting capability of the fuse weakens as it transitions into the second phase, during which the fuse cannot independently make the current reach zero. Thus, the peak of the parameter β was concluded to be the optimal timing to commutate the current.

2.1.3 Workflow of the algorithm

The operation workflow to implement commutation based on the background principle discussed above is presented in Fig.2.4. Initially, the microcontroller unit (MCU) continuously collects the current data on the fuse. The collected data are stored using a sliding window method, which leads the MCU to monitor the current in real-time. Under normal operating conditions within the rated limits, the system is in State 0. During this time, the semiconductor switch remains off and the rated current flows through the fuse with negligible resistance instead of passing through the IGBT.

When consecutive current data exceed the threshold, the system identifies it as a fault condition. Upon detecting the fault, the system moves to State 1.

In State 1, the peak current I_0, as defined in Equation 2.1, is determined by comparing the cumulative sums of the current data at the two ends of the data window. When the cumulative sum of the earlier recorded current data surpasses that of the later recorded data, it indicates that the current has reached its maximum value in the data set and is starting to decline. Once the peak current is detected, the system proceeds to State 2, where the calculation of the β parameter begins.

In State 2, the β parameter is continuously estimated in real-time using the RLS algorithm, as described by Equations 2.3 to 2.6. When the value of β previously calculated exceeds the value of newly calculated, it means that β has peaked during the estimation process. At this point, the system advances to State 3, and the MCU generates a control signal.

This signal activates the IGBTs, starting the current commutation process. After a fixed operating time, the MCU sends a turn-off signal to the IGBTs, shifting the system to State 4 and completing the interruption process.

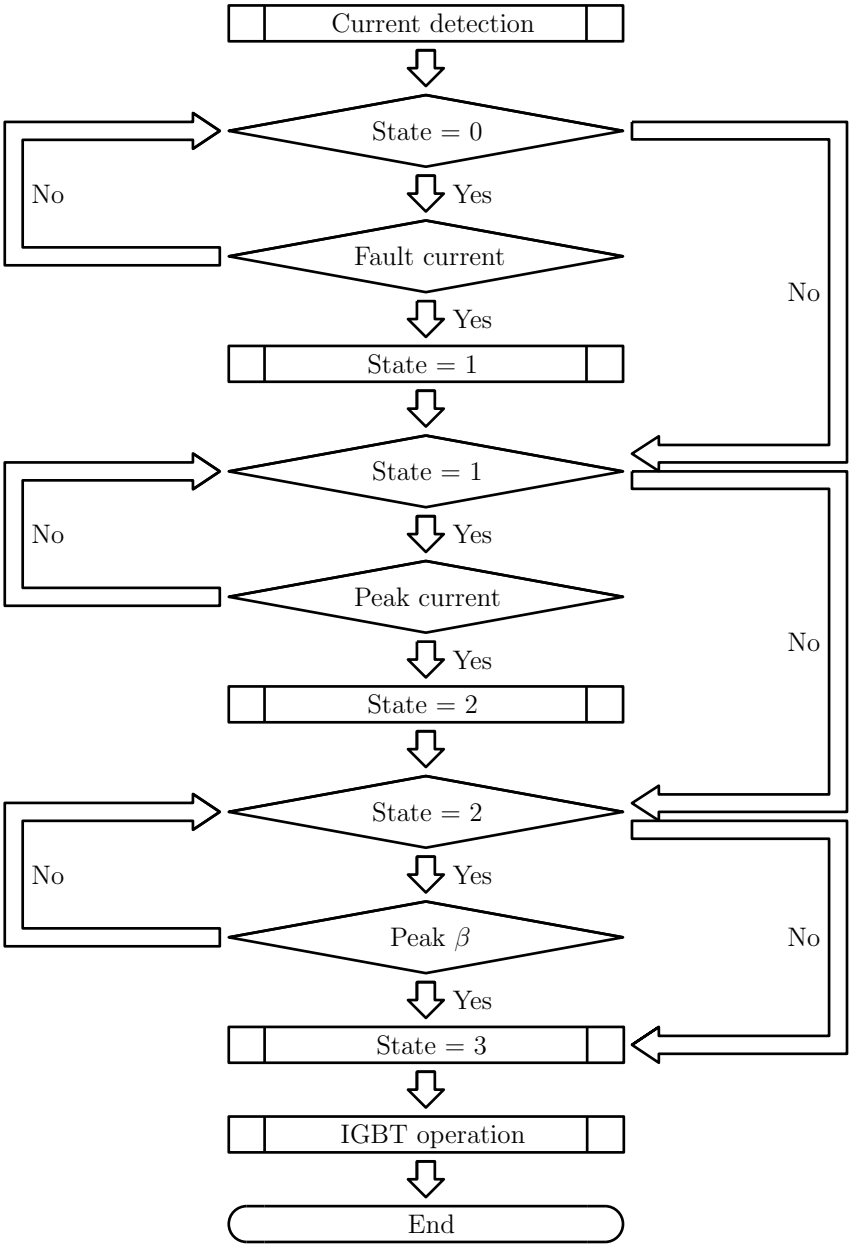

Figure 2.4: The workflow of the current-based commutation operation

The following pseudo-code outlines the implementation of the workflow.

Algorithm 1 Process data for current-based commutation

```
Initialize State, and Current.
if State = 0 then                                   ▷ State 0: Detect Fault
    if Current > FaultThreshold then
        StartTime ← CurrentTime
        PostSurgeData ← CollectData()
        State ← 1
    end if
else if State = 1 then                              ▷ State 1: Detect Peak
    if DetectPeak(PostSurgeData) then
        PeakCurrent ← FindPeak(PostSurgeData)
        PeakTime ← CurrentTime
        State ← 2
    else
        PostSurgeData ← UpdateWindow(Current)
    end if
else if State = 2 then                              ▷ State 2: Perform RLS
    UpdateRLS(Current, PeakCurrent)
    if CommutationConditionMet() then
        TriggerIGBT()
        CommutationTime ← CurrentTime
        State ← 3
    end if
else if State = 3 then                              ▷ State 3: Finalize Data
    if DataCollectionComplete() then
        WriteToSDCard(PostSurgeData)
        State ← 4
    end if
end if
```

2.2 Experimental validation

In previous research by Liu *et al.* [22], the current-based commutation method was tested only once under explosive conditions of 1.5 kV and 5 kA using a ceramic fuse. However, the safety and reliability of the commutation algorithm must be established for practical application. Therefore, this chapter tests the commutation method under various electrical conditions using different types of fuses.

- Fuse explosion experiments
  - Ceramic fuse explosion experiment under 1.7 kV and 10 kA

  - Glass fuse explosion experiment under 0.5 kV

- Validation of current-based commutation using a ceramic fuse
  - 1.7 kV and 10 kA
  - 0.95 kV and 10 kA

- Validation of current-based commutation using a glass fuse

First, fuse explosion experiments were performed. The experiment involved two configurations, one using a ceramic fuse and the other using a glass fuse. Physical changes in the fuses were recorded using a high-speed camera along with current and voltage data measurements. The commutation algorithm was then tested under higher voltage and current conditions such as 1.7 kV and 10 kA with a ceramic fuse. Additional tests with the same fuse were performed at 0.95 kV and 10 kA. Finally, a glass fuse was used to further validate the reliability of the algorithm under conditions of 0.4 kV and 0.5 kA.

2.2.1 Experimental setup

The fuse explosion experiment involves only the fuse itself, which does not require additional explanation. Therefore, this section focuses on introducing the experimental setups for the other tests.

The experimental circuit diagram of the fuse-semiconductor hybrid DC circuit breaker used to validate the current-based commutation algorithm is shown in Fig.2.5.

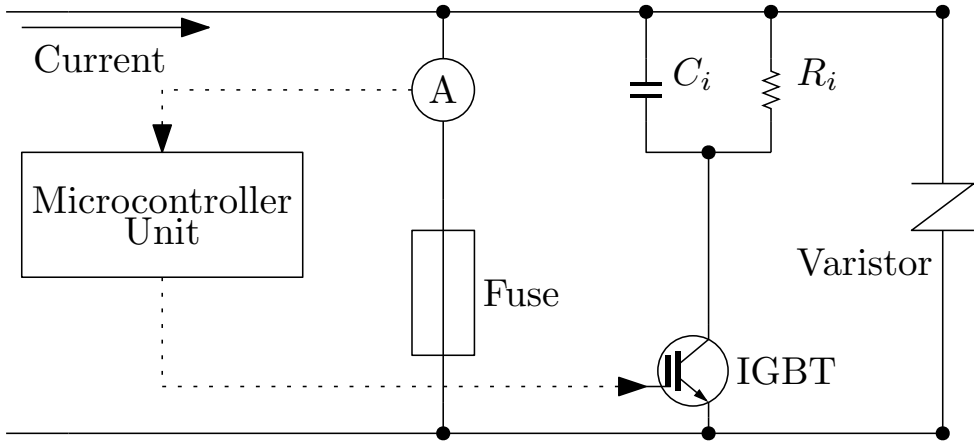

Figure 2.5: Circuit diagram for the current-based commutation validation experiment

The test circuit consists of a fuse in the main branch, an IGBT in the secondary branch, and MOVs in the third branch. In addition, the circuit includes a resistor connected in parallel with a capacitor. A Rogowski current sensor with a 2000:1 scaling ratio is placed in the fuse branch, and the measured current data is sent to the MCU. In this experiment, Teensy 4.1 is used as the MCU due to its cost efficiency, compact size, and fast computational capabilities. An additional parallel RC circuit is connected near the IGBT to protect it from malfunctions caused by rapid current surges and high voltage.

The MCU receives the measured current data through its General Purpose Input/Output (GPIO) port at a sampling frequency of 50 kHz. A basic window size of 50 was used, with fault current detection performed using 30 data points. The peak current was identified using a window size of 20, where three consecutive data points from each end of the peak window were compared. To minimize the impact of noise, the forgetting factor (λ) was set at 0.97.

For the fuse explosion tests, the ceramic fuse with a rated voltage of 1 kV and a rated current of 50 A was used. It was tested under conditions of 1.7 kV and 10 kA. Similarly, the glass fuse, with a rated voltage of 250 V and a rated current of 0.63 A, was tested under 0.5 kV. In the second experiment using the same ceramic fuse, tests were conducted at 1.7 kV and 10 kA, as well as 0.95 kV and 10 kA. Finally, the glass fuse was tested again under the same conditions of 400 V and 500 A.

For the experiment using a ceramic fuse, the parallel RC circuit on the IGBT branch consists of a 10 Ω resistor in parallel with a 642 μF capacitor. For the experiment using a glass fuse, the resistor is replaced with a 0.5 Ω resistor. When the current path switches to the IGBT branch, the capacitor initially offers very low impedance, much lower than that of the fuse, allowing the current to transition smoothly to the IGBT branch. As the reactance of the capacitor increases with time, the current begins to flow through the resistor, which still provides lower resistance than the fuse. This keeps the continuous current flowing through the IGBT branch while protecting the IGBT from excessive current and voltage.

2.2.2 Experimental results

- Fuse explosion experiments
  - Ceramic fuse explosion experiment under 1.7 kV and 10 kA

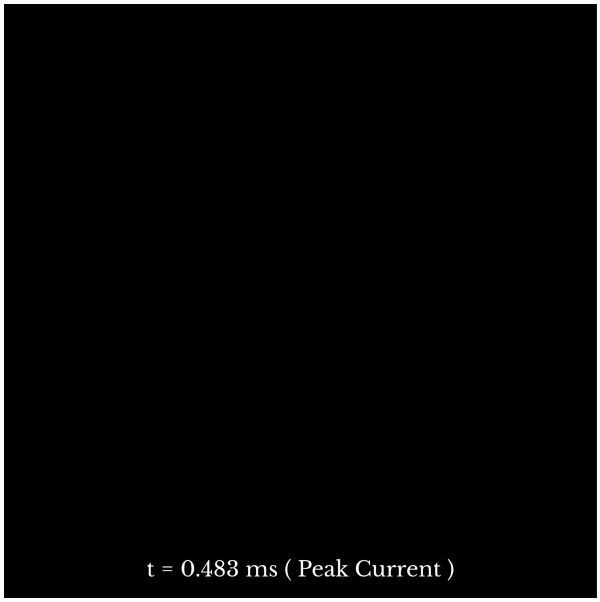

(a) Ceramic fuse status at the peak current point

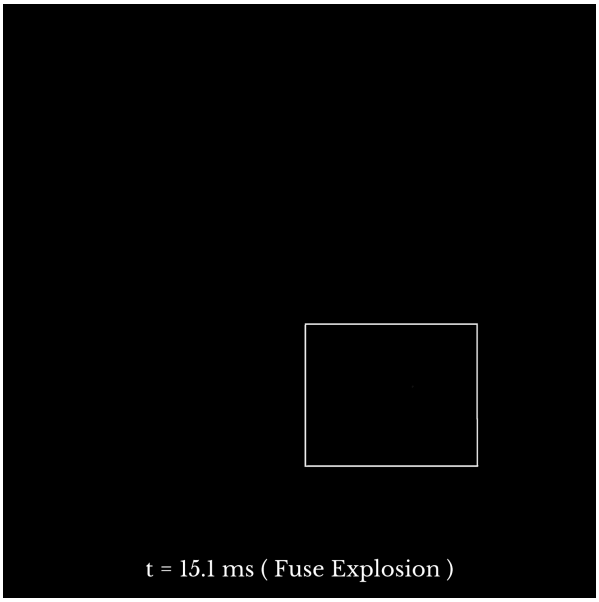

(b) Ceramic fuse status at the onset of explosion

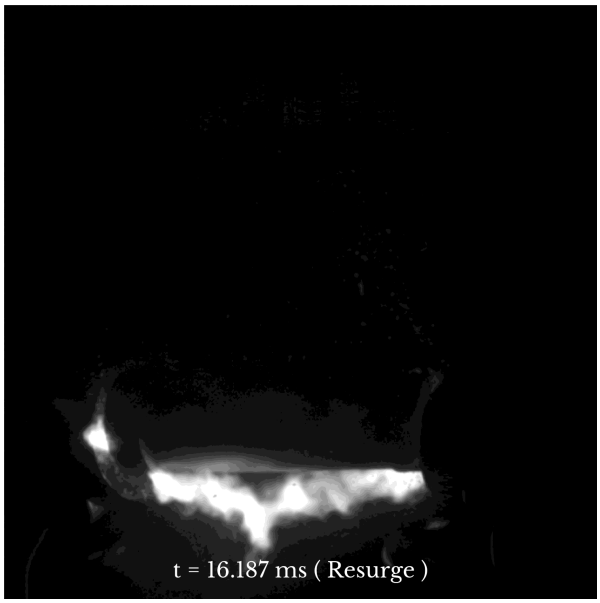

(c) Ceramic fuse status at the onset of current resurge

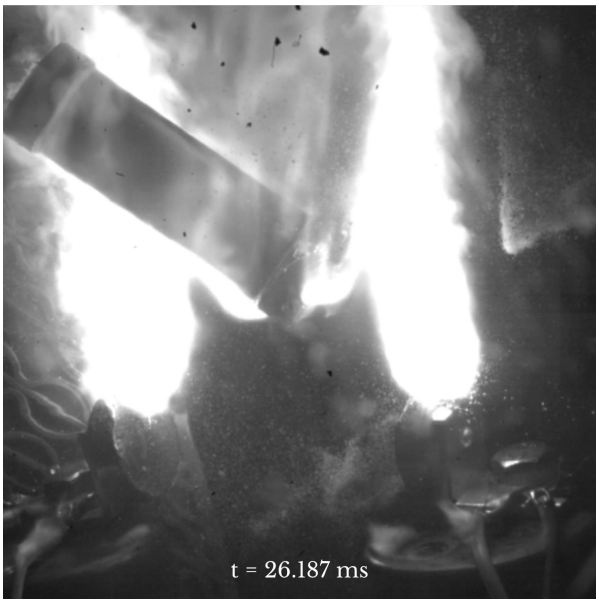

(d) Ceramic fuse status after 10 ms from the current resurge

Figure 2.6: Change in ceramic fuse status under 1.7 kV and 10 kA

To observe the physical state changes of the ceramic fuse, a high-speed camera recorded the fuse in real-time while simultaneously capturing current and voltage data. Fig.2.6 presents images of the fuse at specific moments, which are compared with the corresponding electrical data shown in Fig.2.7.

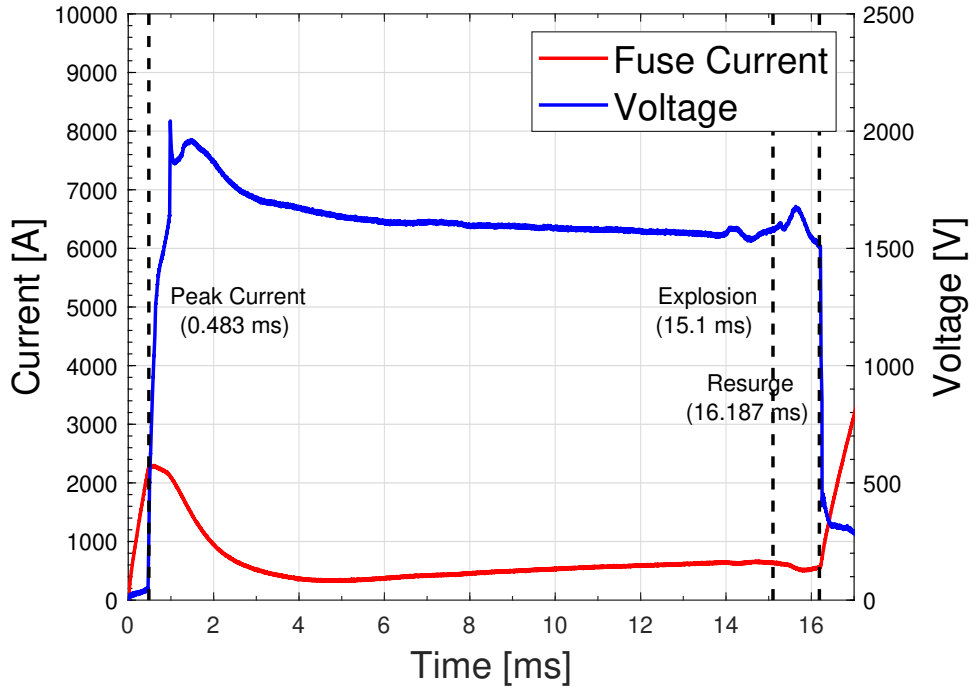

Figure 2.7: Current and voltage data of the ceramic fuse under 1.7 kV and 10 kA

The arcing phase begins with a voltage surge at $t = 0.483$ ms. During this moment, no visual changes are captured by the high-speed camera due to the casing of the fuse. At $t = 15.1$ ms, a small light becomes visible in the camera. In this context, the explosion of the ceramic fuse is identified as the moment when light is captured first by the camera. Therefore, this moment marks the start of the explosion of the ceramic fuse. Although the explosion is visually evident in the camera, the current and voltage data shown in Fig.2.7 indicate that the system is still in the second phase, as defined in Section 2.1.1, where a low current continues to flow.

As the current begins to resurge at $t = 16.187$ ms in the recorded data, the current passing through the external arc of the fuse becomes more apparent, as depicted in Fig.2.6c. Subsequently, Fig.2.6d presents the fuse status 10 ms after the resurge event. Finally, the condition of the fuse at the end of the explosion test is shown in Fig.2.8. From this image, the light observed in Fig.2.6d is interpreted as fire. This experiment reveals that the physical explosion of the fuse does not coincide with the current surge.

Figure 2.8: Post-test condition of the ceramic fuse

- Fuse explosion experiments
  - Glass fuse explosion experiment under 0.5 kV

Basically, the ceramic current-limiting fuse is made of a thin wire or ribbon element coil, which is called a fuse link around a form and enclosed in an insulating ceramic tube filled with sand [28, 29]. On the other hand, the glass fuse is encased in a transparent glass tube, which does not contain additional material inside [30].

In this experiment, a glass fuse with a rated voltage of 250 V and a rated current of 0.63 A was used. Separate explosion experiments were conducted for the glass and ceramic fuses because of their distinct structures and components, which are expected to exhibit different characteristics. Additionally, the transparent tube of the glass fuse allows for a clearer observation of the status of the fuse.

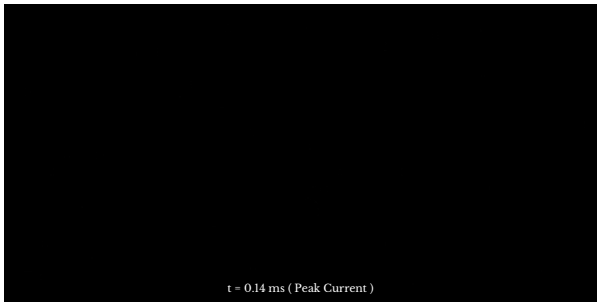

(a) Glass fuse status at the peak current point

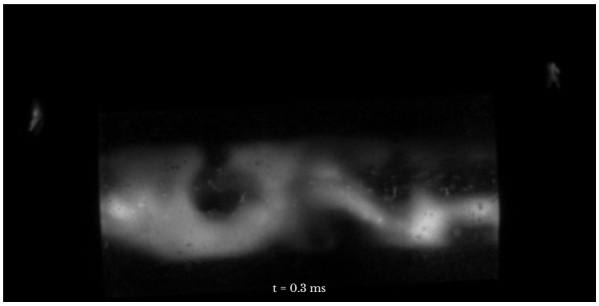

(b) Glass fuse status at the first resurge

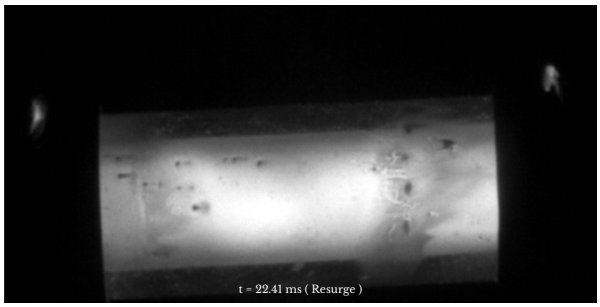

(c) Glass fuse status at the second resurge

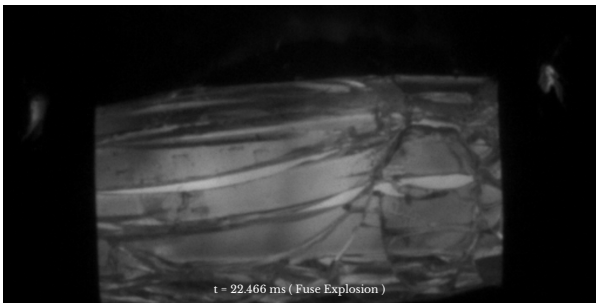

(d) Glass fuse status at the onset of explosion

Figure 2.9: Change in glass fuse status under 0.5 kV

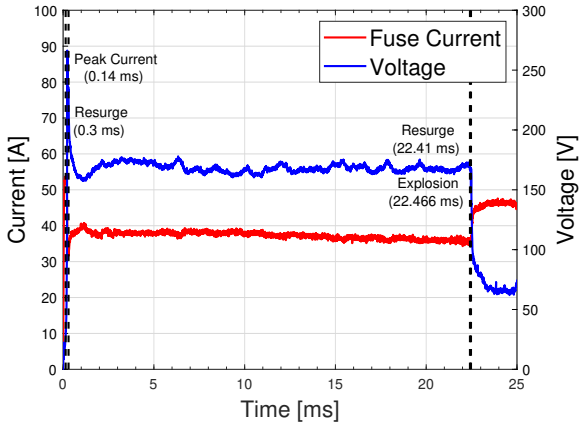

(a) Current and voltage data of the glass fuse under 0.5 kV for 25 ms

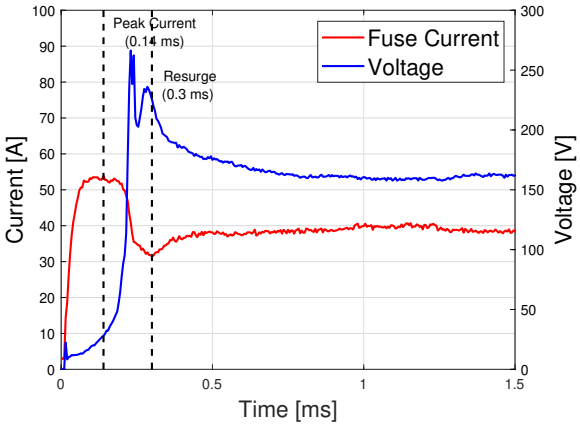

(b) Current and voltage data of the glass fuse under 0.5 kV for 1.5 ms

Figure 2.10: Current and voltage data of the glass fuse under 0.5 kV

The status of the glass fuse during the explosion is shown in Fig.2.9. The corresponding current and voltage waveforms are presented in Fig.2.10a. At $t = 0.14$ ms, the current peaks with a surge in voltage that marks the beginning of the arcing phase. During this phase, the current flows through the internal fuse link, and no visible changes are observed in Fig.2.9a.

Different characteristics of the glass fuse waveform appear in the zoomed plot in Fig.2.10b. Unlike the ceramic fuse, where the arcing current has a smooth curve before the resurge, the glass fuse shows a resurge shortly after rapid current limitation. This resurgence occurs at $t = 0.3$ ms and is captured in Fig.2.9b. A second resurge occurs at $t = 22.41$ ms just before the explosion. At this point, the arc fills the entire glass tube as shown in Fig.2.9c. At $t = 22.466$ ms the glass fuse explodes. The explosion is defined as the moment the glass tube fractures.

The following figure shows the glass fuse after the experiment. Due to the high pressure and energy generated during the explosion, only the metal cap remains. This demonstrates how a fuse explosion can pose a serious danger to the entire system.

Figure 2.11: Post-test condition of the glass fuse

- Validation of current-based commutation using a ceramic fuse
  - 1.7 kV and 10 kA

The current-based fuse state estimation is validated in this experiment using a ceramic fuse under explosive conditions of 1.7 kV and 10 kA. Fig.2.12 shows the current and voltage waveforms observed during the current interruption process. The fault current is initiated at $t = 0$ ms and increases to 2.3 kA by $t = 0.51$ ms. When the current peaks, the fuse link ignites, producing an arc voltage that signifies the start of the arcing phase. Subsequently, the current decreases

rapidly until $t = 2.1$ ms. At this point, the current path is switched from the fuse to the IGBT branch by turning on the IGBT.

The IGBT is turned off at $t = 7.394$ ms, completing the current interruption process in the fuse-semiconductor hybrid DC circuit breaker. The IGBT is set to remain active for 5 ms to ensure sufficient insulation of the fuse and prevent re-arcing. However, due to the current tailing characteristic of the IGBT, the interruption is delayed by a few microseconds [31]. During IGBT operation, the current through the IGBT path initially increases briefly because of the low resistance. The current then decreases and stabilizes at approximately 173 A. A similar effect occurs when the IGBT is turned off as the varistors absorb the residual energy.

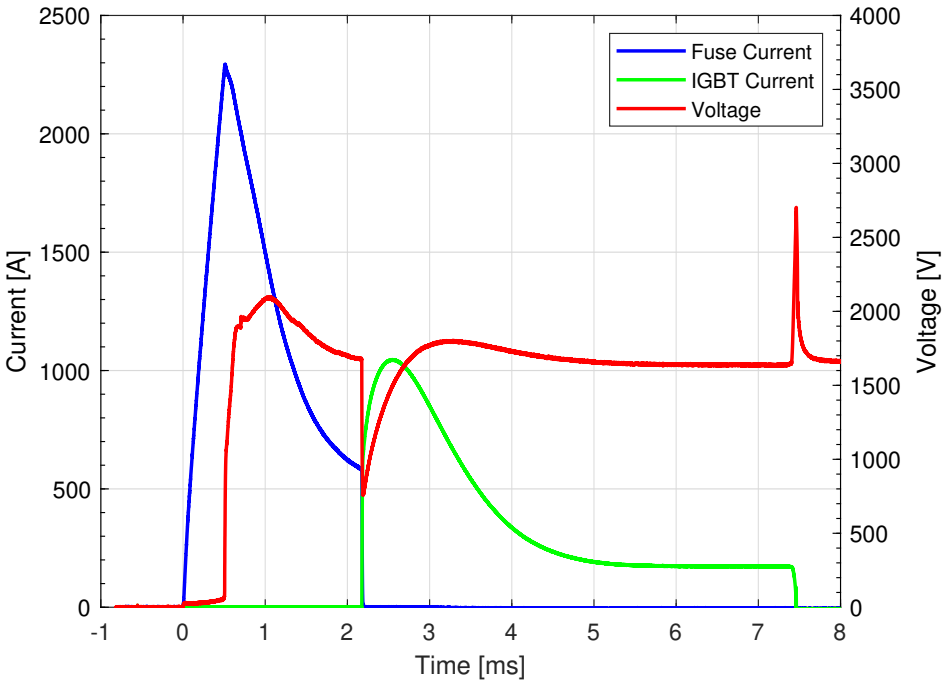

Figure 2.12: Current and voltage waveforms in current-based commutation experiment using a ceramic fuse under 1.7 kV and 10 kA

To initiate the IGBT operation, the MCU monitors the current data in real-time and calculates the β value, which represents the dynamic $\frac{1}{R_{\text{arc}}C_{\text{arc}}}$ to model the arcing current. The recorded β value is shown in Fig.2.13. At $t = 0.74$ ms, the β value calculation begins. The gap between the peaks observed in Fig.2.12 and in Fig.2.13 occurs because the algorithm uses a sliding window method, which requires a specific amount of data to identify the maximum current. The calculated β value increases until $t = 2.1$ ms, and a signal is sent to the IGBT. It was observed

that the GPIO signal from the MCU activates the IGBT immediately, without delay.

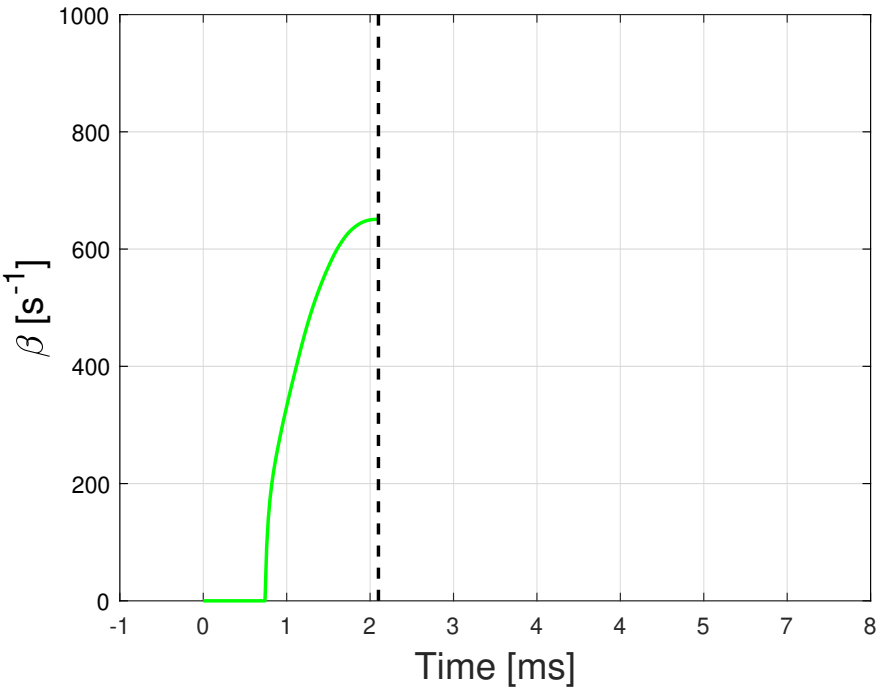

Figure 2.13: β value calculated and recorded in MCU (Teensy 4.1) under 1.7 kV and 10 kA conditions

- Validation of current-based commutation using a ceramic fuse
  - 0.95 kV and 10 kA

In this experiment, the same ceramic fuse was tested for current-based fuse state estimation at a voltage of 0.95 kV. Fig.2.14 shows the current and voltage waveforms recorded during the experiment. The waveforms are similar to those observed in the previous experiment conducted at 1.7 kV. The peak current is approximately 1.9 kA and is detected at $t = 0.75$ ms, where the arc channel forms as the fuse metal link melts. As the gap in the fuse link widens, the plasma channel weakens, reducing the current flow [24]. At $t = 2.214$ ms, the IGBT is activated and the current decreases from 0.27 kA to zero. The current path is successfully transferred to the semiconductor branch. After 5 ms, the IGBT is turned off, completing the operation at $t = 7.482$ ms

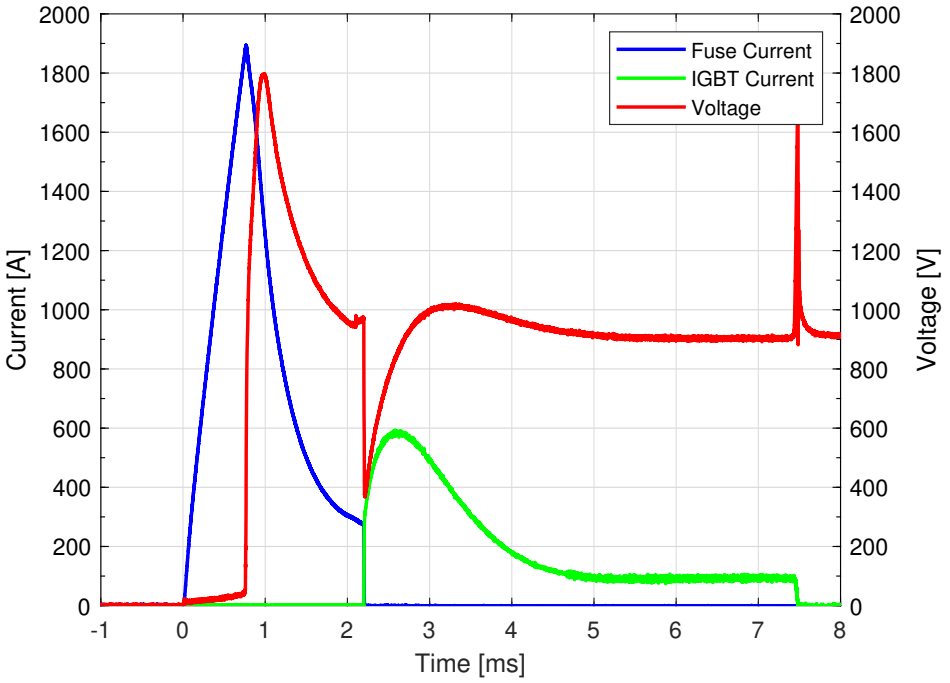

Figure 2.14: Current and voltage waveforms in current-based commutation experiment using a ceramic fuse under 0.95 kV and 10 kA

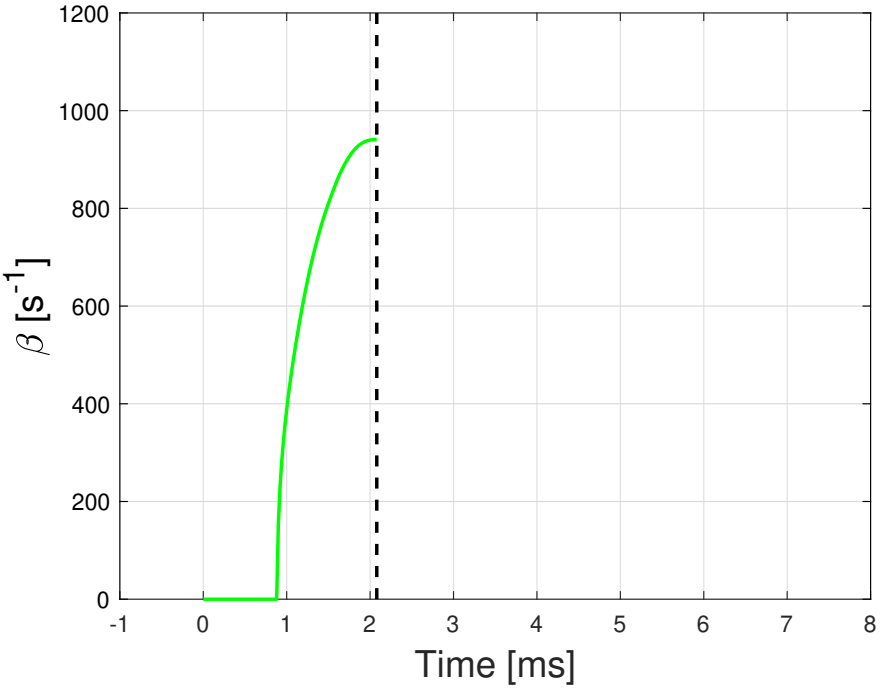

Figure 2.15: β value calculated and recorded in MCU (Teensy 4.1) under 0.95 kV and 10 kA conditions

Fig.2.15 shows the calculated data to determine the commutation time. The parameter β was calculated from $t = 0.88$ ms. Its value was increased until $t = 2.1$ ms, where the maximum value β was identified. Based on this calculation, a control signal is sent to the IGBT via GPIO. At this point, the on-state resistance of the IGBT is lower than that of the fuse, allowing the current to flow through the IGBT branch.

- Validation of current-based commutation using a glass fuse

To observe internal changes and verify the algorithm's performance in various situations, a glass fuse was used in this experiment. The experiment was performed at 0.4 kV and 0.5 kA. Fig.2.16 shows the current and voltage waveforms during the experiment. A unique characteristic of the glass fuse's current waveform is visible in the figure. The maximum current during the arcing process occurred at $t = 3.97$ ms, after a 2.5 ms delay from the pre-arcing peak current. The IGBT was turned on at $t = 6.04$ ms and turned off at $t = 11.45$ ms, 5 ms later.

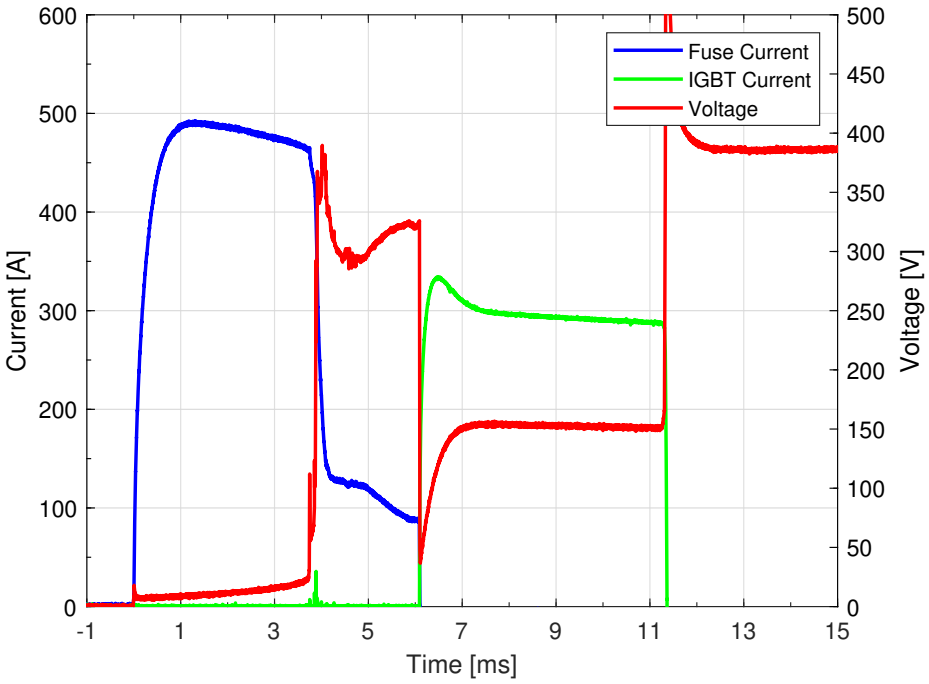

Figure 2.16: Current and voltage waveforms in current-based commutation experiment using a glass fuse under 0.4 kV

Fig.2.17 shows the β calculation for this experiment. Based on the characteristic of the current waveform in Fig.2.16, the β value was calculated from $t = 1.4$ ms, much earlier than the

actual peak of the arcing current. In this situation, the pre-arcing peak current was identified as the peak, and due to the sliding-window method's delay, the β calculation for State 2 started at this point. The limitations of this situation will be discussed in the next section. After starting the calculation, the value of β remained small until the arcing process began at $t = 3.97$ ms. The β value reached its peak at $t = 6.04$ ms, when the signal was sent.

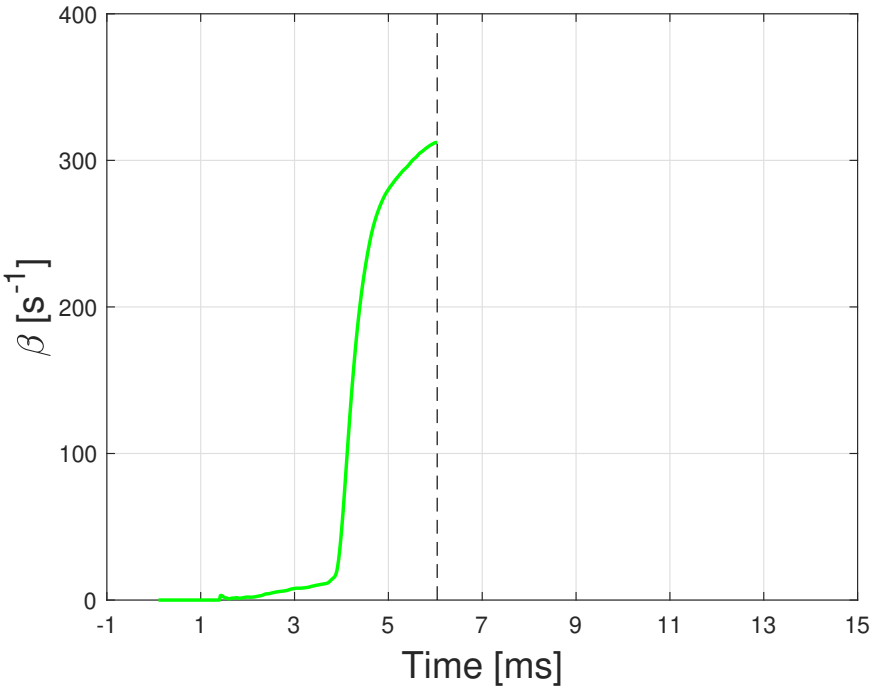

Figure 2.17: β value calculated and recorded in MCU (Teensy 4.1) under 0.4 kV and 0.5 kA conditions

The following figure depicts the internal change of the glass fuse during the commutation process. When the arc formed at $t = 3.97$ ms, the light started from the fuse cap and followed the fuse metal link. At $t = 6.04$ ms, when the MCU sent the operating signal, the arc filled the fuse glass tube. A much weaker arc was shown in Fig.2.18c, after 0.5 ms from IGBT activation. This indicates that the commutation effectively switched the fuse current to the IGBT, preventing an explosion. After 3 ms, it is observed that the arc disappeared completely.

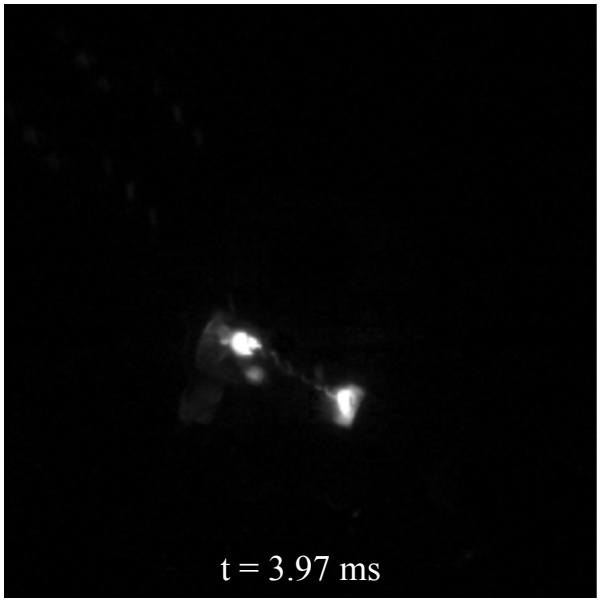

(a) Glass fuse status at the peak current

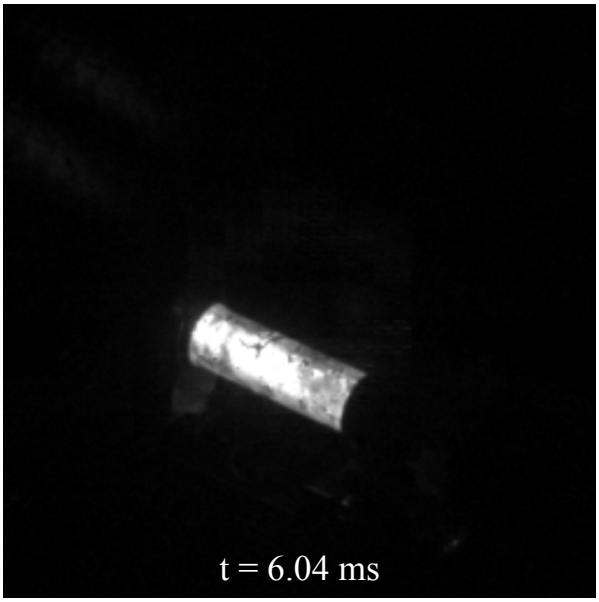

(b) Glass fuse status at the commutation initiation

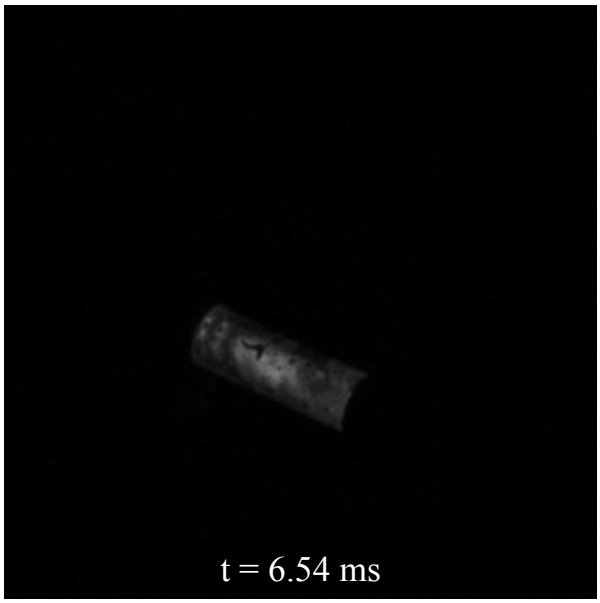

(c) Glass fuse status after 0.5 ms from the commutation initiation

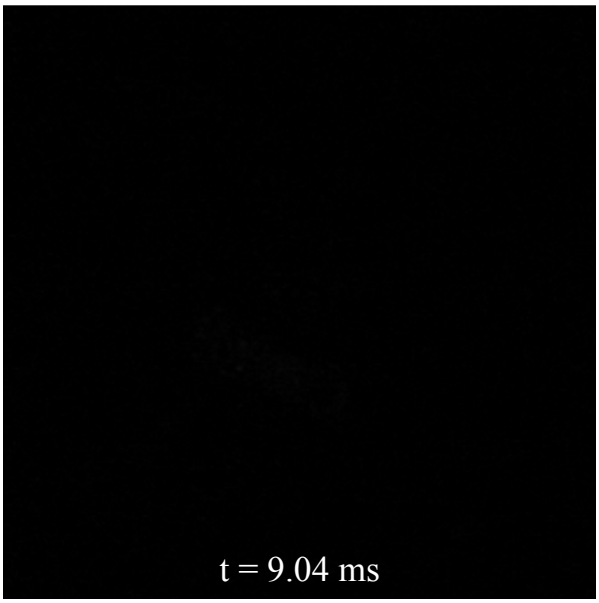

(d) Glass fuse status after 3 ms from the commutation initiation

Figure 2.18: Change in glass fuse status under 0.4 kV with the current-based commutation method

The glass fuse after the commutation experiment is shown in Fig.2.19. Compared to Fig.2.11, the glass tube remained intact. The brown residue on the tube was caused by the high energy and heat generated by the arc.

Figure 2.19: Post-commutation condition of the glass fuse

2.3 Discussion

In the previous section, the current-based fuse state estimation method for determining the commutation time was validated under various conditions. Based on these experimental results, this section discusses the analysis and limitations of the current-based method.

2.3.1 Analysis of the current-based commutation

First, the arcing current is modeled as follows in the current-based method:

$$i(t) = I_0 \cdot e^{\frac{-t}{R_{\text{arc}} C_{\text{arc}}}} \tag{2.7}$$

$$= I_0 \cdot e^{-\beta t} \tag{2.8}$$

The method identifies the optimal commutation time when $\frac{1}{R_{\text{arc}} C_{\text{arc}}}$, defined as the β parameter, reaches its peak value. The β parameter is expressed using Equation 2.7 as follows:

$$\frac{di(t)}{dt} = I_0 \cdot (-\beta) \cdot e^{-\beta t} \tag{2.9}$$

$$\beta = -\frac{\frac{di(t)}{dt}}{i(t)} \tag{2.10}$$

To find when β reaches its maximum value, the first-order derivative of β is given as:

$$\frac{d\beta}{dt} = -\frac{i(t) \cdot \frac{d^2 i(t)}{dt^2} - \left(\frac{di(t)}{dt}\right)^2}{i(t)^2} \tag{2.11}$$

There are two cases where β reaches its peak, and the first is shown below:

$$\frac{di(t)}{dt} = 0 \tag{2.12}$$

From Equation 2.12, β reaches its peak before the current gradient becomes zero. During the arcing phase, β is positive until the current rises again. If Equation 2.12 is satisfied, β becomes zero according to Equation 2.10. Therefore, the peak occurs just before this moment. This case usually occurs in the glass fuse current waveform, where two current resurges are present, as shown in Fig.2.10.

The second case occurs when the first- and second-order derivatives of the current satisfy a specific ratio:

$$\frac{\frac{d^2i(t)}{dt^2}}{\frac{di(t)}{dt}} = \frac{\frac{di(t)}{dt}}{i(t)} \tag{2.13}$$

This situation is common in ceramic fuses, where the current waveform during arcing is smooth.

The parameter β in this situation can be understood as the stability of the current system, as shown below:

$$I(s) = \frac{I_0}{s + \beta} \tag{2.14}$$

An increase in β indicates that the current system converges more rapidly, meaning that the fuse's limiting ability is still effective. On the other hand, a decrease in β shows slower current convergence, which implies that the fuse's limiting ability is weakening. From this perspective, the peak value of β represents the optimal moment for commutation.

2.3.2 Limitations of the current-based commutation

Although the current-based commutation method works in various situations, some limitations are still observed in the experiments.

- Gap between the physical phenomena and current data

Table 2.1 compares the actual resurge and explosion times under various conditions. The resurge and explosion times are close but not exactly the same. In the third case, the explosion occurred more than 2 ms earlier than the resurge. This shows that relying only on current data is not accurate enough.

Table. 2.1: Resurge and explosion times under different conditions

Fuse type (rated value)	**Condition**	**Resurge (ms)**	**Explosion (ms)**
Ceramic (1 kV, 50 A)	1.7 kV	16.19	15.10
Glass (250 V, 0.63 A)	500 V	22.41	22.47
Glass (250 V, 10 A)	400 V	11.18	8.70

- Delay in sending the signal to IGBT

There is a delay between the simulation and the experiment. Fig.2.20 presents the results of the algorithm simulation. According to Equation 2.9, the signal should be triggered when the current gradient changes from negative to positive. In the simulation, the commutation is determined at the moment when the first-order derivative of the current becomes zero.

However, as shown in Fig.2.21, the experiment demonstrates that commutation occurs at $t = 0.967$ ms, with a delay of 0.772 ms from the first resurgence. This delay arises because the RLS algorithm relies on past data, making it sensitive to the sampling frequency. Furthermore, the maximum MCU processing frequency is constrained in real-time applications, causing a gap between the simulation and experimental results.

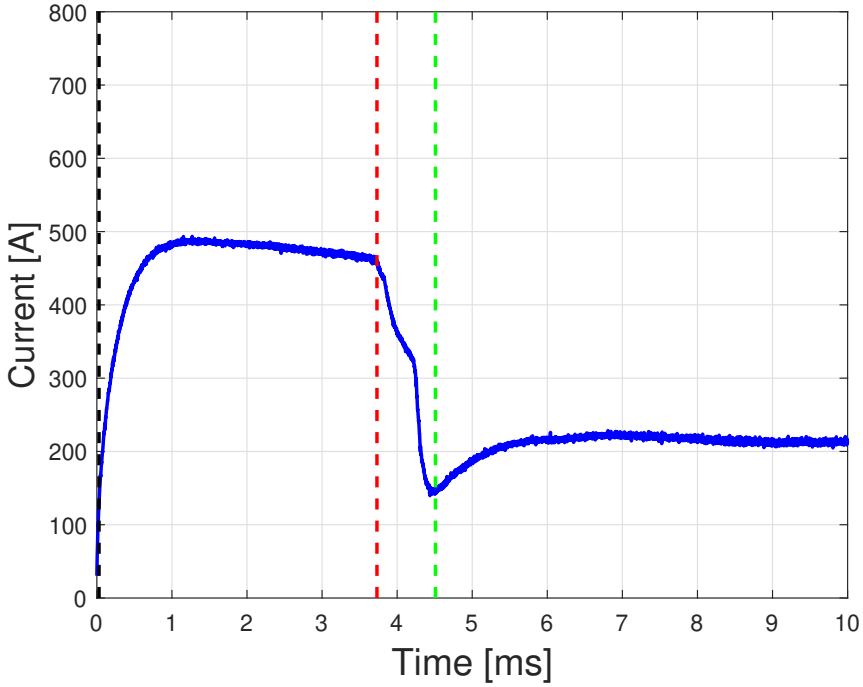

Figure 2.20: Current-based commutation simulation using glass fuse data

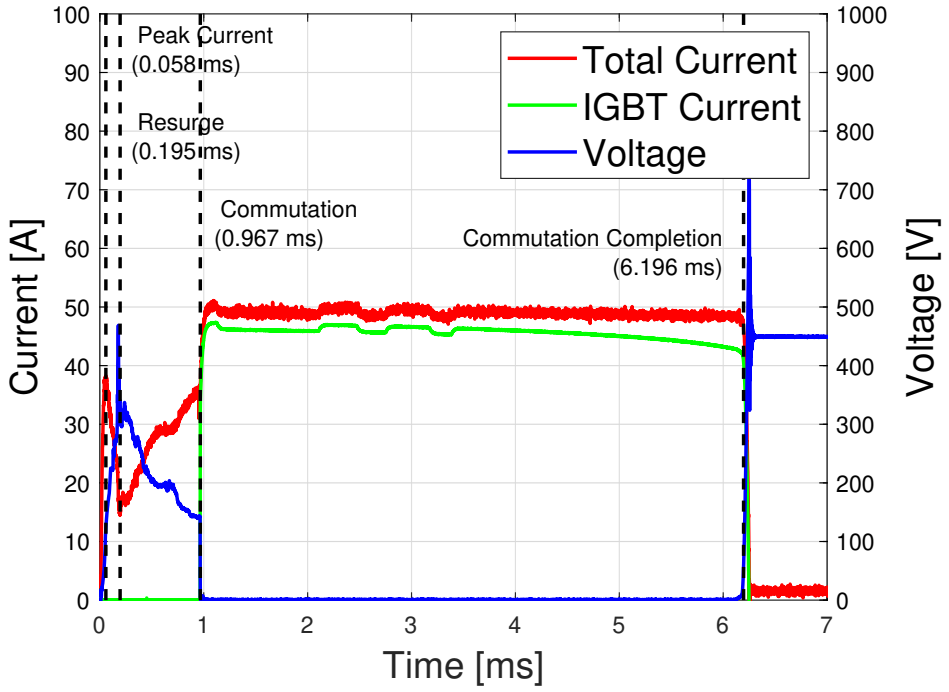

Figure 2.21: Commutation delay observed in the experiment with a glass fuse

- Premature commutation error

As described in Section 2.2.2, the β value can be calculated before the arcing phase begins. This may lead to premature commutation, where the fault current is switched to the IGBT before it is sufficiently limited for interruption.

Fig.2.22 presents the experimental results when the pre-arcing current peak occurs separately from the arcing current peak. In this case, the β parameter starts to be calculated from the pre-arcing peak, causing the IGBT signal to be sent prematurely at $t = 5.455$ ms. Consequently, the IGBT was unable to interrupt the fault current.

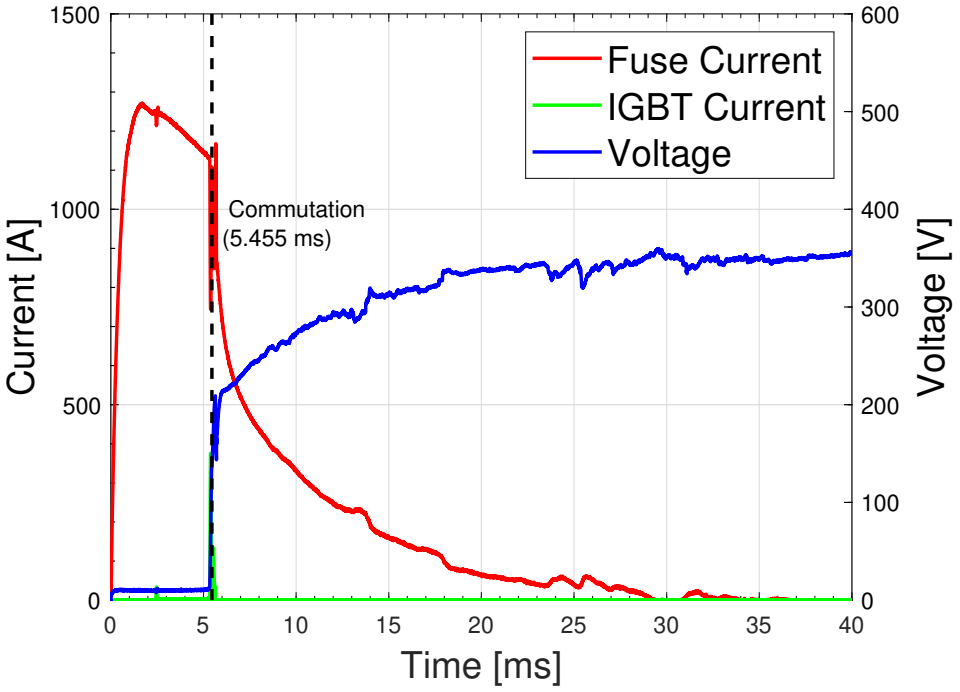

Figure 2.22: Premature commutation error in experiment

- Commutation operation when fuse-only interruption is feasible

Lastly, in some cases, current-based commutation is activated even when the fuse alone can fully interrupt the fault current. This adds extra operating time for the IGBT. As a result, the overall interruption process of the hybrid DC CB is delayed. Such delays affect an important factor in evaluating the performance of the DC CB.

Chapter 3

Proposal and experimental validation of current-voltage-based commutation

To overcome the limitations mentioned in the previous chapter 2.3.2, this chapter proposes a current-voltage-based method to initiate the commutation. Specifically, the energy criterion is applied to determine the commutation time.

3.1 Energy threshold calculation based on the simulation

In Fig.2.1, the fuse status was divided into three phases. Under explosive conditions, different waveform characteristics appear in the second phase, and the fuse explodes in the third phase. The goal of sequence control using the commutation method is to identify the optimal time to change the current path after the fuse has efficiently limited the energy but before it explodes.

Fig.3.1 shows the peak current moment and the current resurge under conditions of 1.7 kV and 10 kA, which are explosive. The current-based fuse state estimation analyzes these current data. To determine a more precise commutation time while considering the fuse's current-limiting capability, minimum and maximum energy thresholds are calculated.

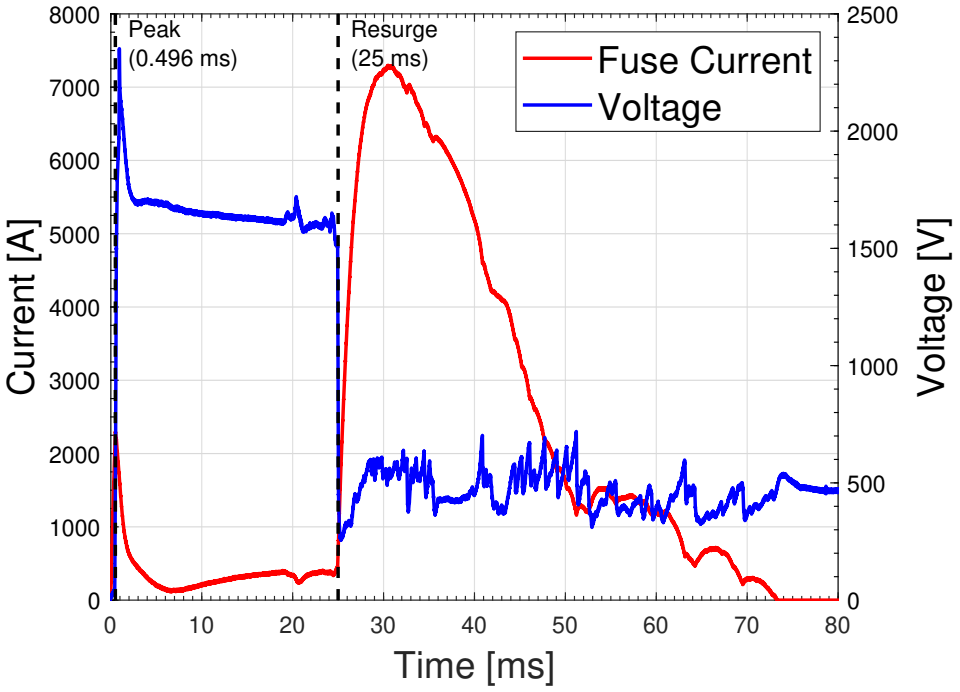

Figure 3.1: Current and voltage waveforms under explosive conditions

3.1.1 Minimum energy threshold calculation

This section begins with a brief recap of Section 2.1.2. In that section, the discharging RC circuit was introduced as the arc current model proposed by Tanaka *et al.* [25] and Li *et al.* [26]. In their studies, $\frac{1}{R_{\text{arc}}C_{\text{arc}}}$ was empirically derived. However, under explosive conditions, a single fixed value of $\frac{1}{R_{\text{arc}}C_{\text{arc}}}$ cannot accurately model the system, as shown in Fig.2.3. This limitation led to the introduction of the RLS algorithm in current-based commutation [22] to estimate the dynamic $\frac{1}{R_{\text{arc}}C_{\text{arc}}}$.

This implies that if the real-time energy of the fuse exceeds the energy limit modeled by a single $\frac{1}{R_{\text{arc}}C_{\text{arc}}}$, it may indicate the scenario in which the fuse cannot interrupt the fault current independently. Therefore, the initial $\frac{1}{R_{\text{arc}}C_{\text{arc}}}$ derived from previous explosive data is used to calculate the minimum energy threshold.

Fig.3.2 shows the current and voltage of the fault when the fuse perfectly limits the current under a 100 V condition. The green line is the modeled arcing current using the initial value of $R_{arc}C_{arc}$, and at this time the saturated energy gap is 2.345 J, which is about 4.5 % difference from the real cumulated energy. This result shows that the minimum energy threshold, which

is the energy accumulated when the fuse can stop the fault current, can be obtained using the initial value $R_{arc}C_{arc}$.

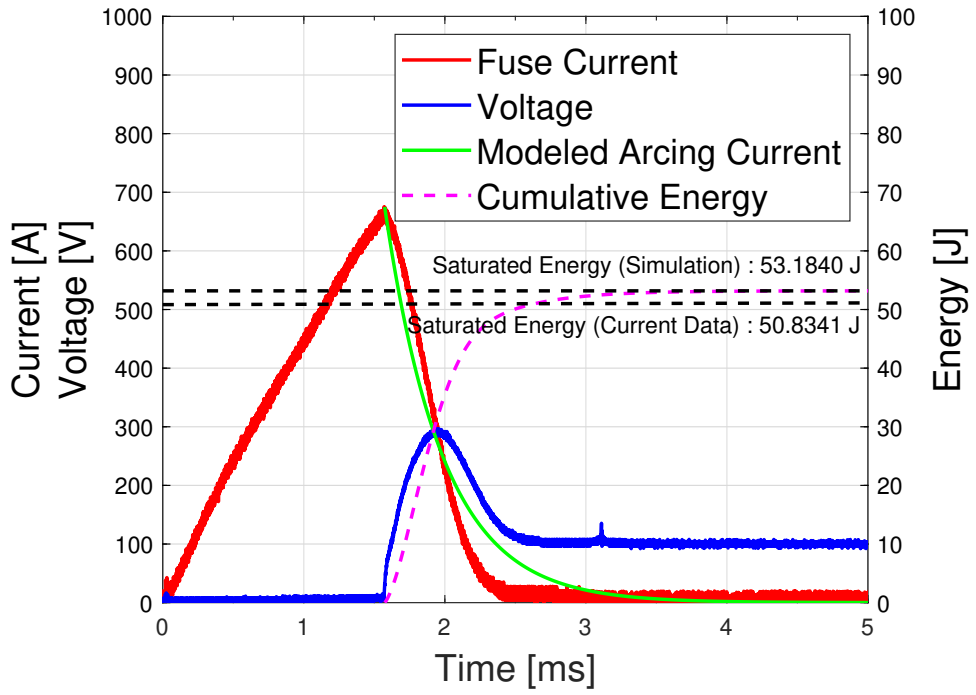

Figure 3.2: Arcing current model and fully interrupted fuse current showing 4.5 % energy calculation error at 100 V

- Simulation of the minimum energy threshold for a ceramic fuse

Based on the simulation results shown in Fig.3.2, the minimum energy threshold is calculated using explosive data obtained previously for a ceramic fuse and a glass fuse, respectively.

Fig.3.3 presents the simulation of the minimum energy threshold for a ceramic fuse. Following the procedure described in the previous paragraph, the arcing current is derived using the initial $\frac{1}{R_{\mathrm{arc}}C_{\mathrm{arc}}}$ and the peak current during the arcing phase. The cumulatively calculated energy, based on the modeled arcing current and voltage data from the peak current ($t = 0.496\,\mathrm{ms}$), is shown as a purple dotted line. The energy saturates at 3.852 kJ.

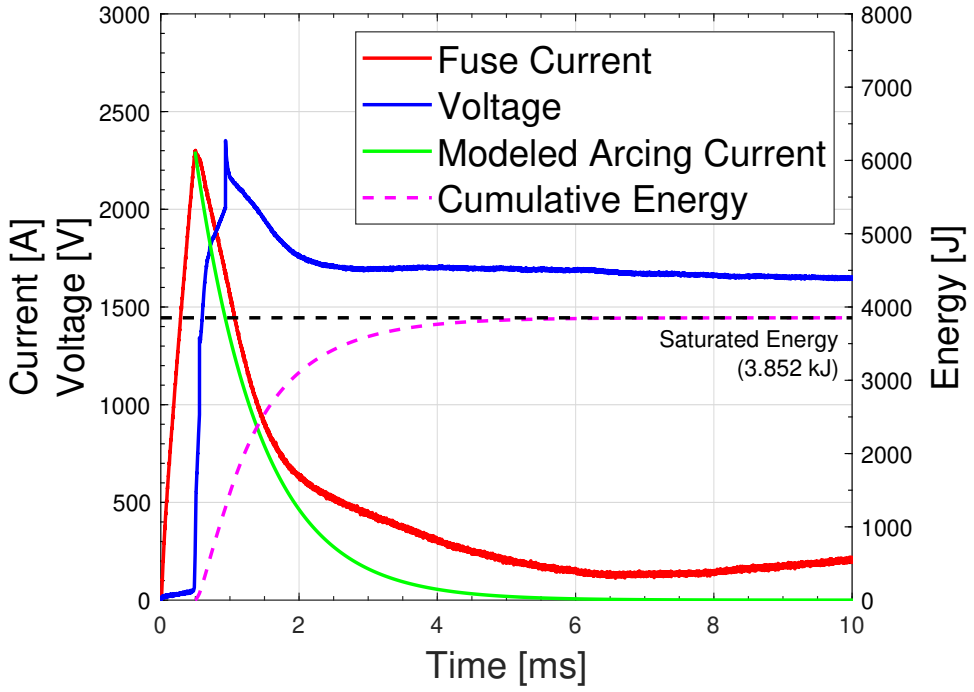

Figure 3.3: Arcing current model and minimum energy threshold of a ceramic fuse under explosive conditions

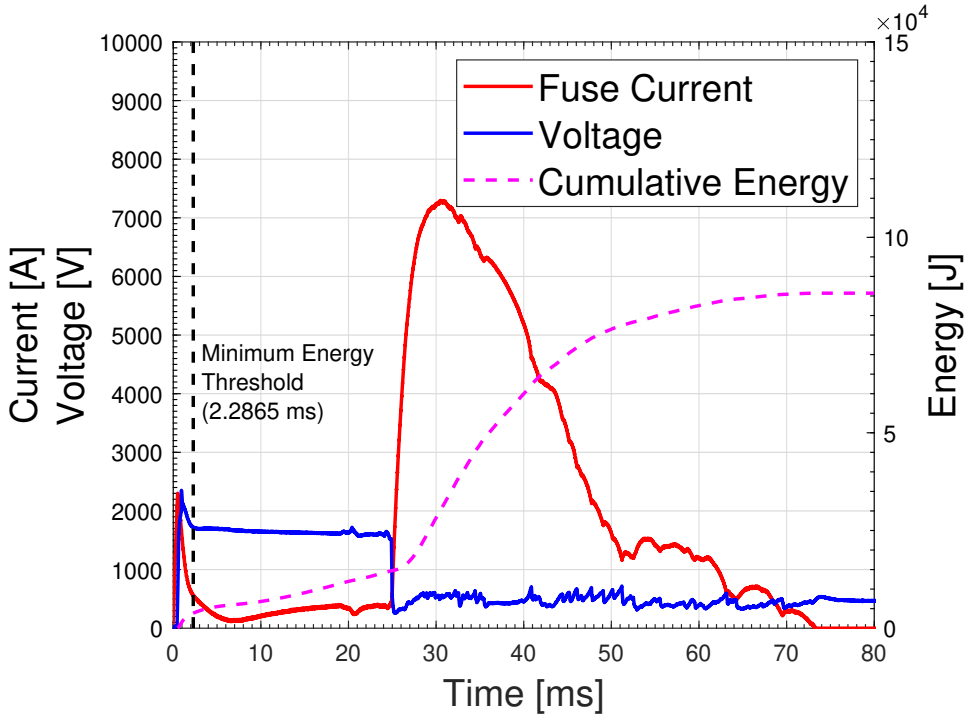

Figure 3.4: Estimated time to reach the minimum energy threshold in a ceramic fuse explosion test

Fig.3.4 illustrates the estimated time at which the cumulative energy reaches the minimum energy threshold from the previous experiment. At $t = 2.2865$ ms, the fuse energy exceeds the minimum energy threshold, indicating that the fuse cannot interrupt the fault current on its own under this condition.

- Simulation of the minimum energy threshold for a glass fuse

The same simulation is conducted for a glass fuse.

Fig.3.5 depicts the simulated minimum energy threshold with the arcing current model. In this simulation, the energy saturates at 52.6405 J, which is reached during the explosion test at $t = 4.855$ ms, as shown in Fig.3.6. The minimum energy threshold is applied after the first resurge, but before the current saturates in the second phase.

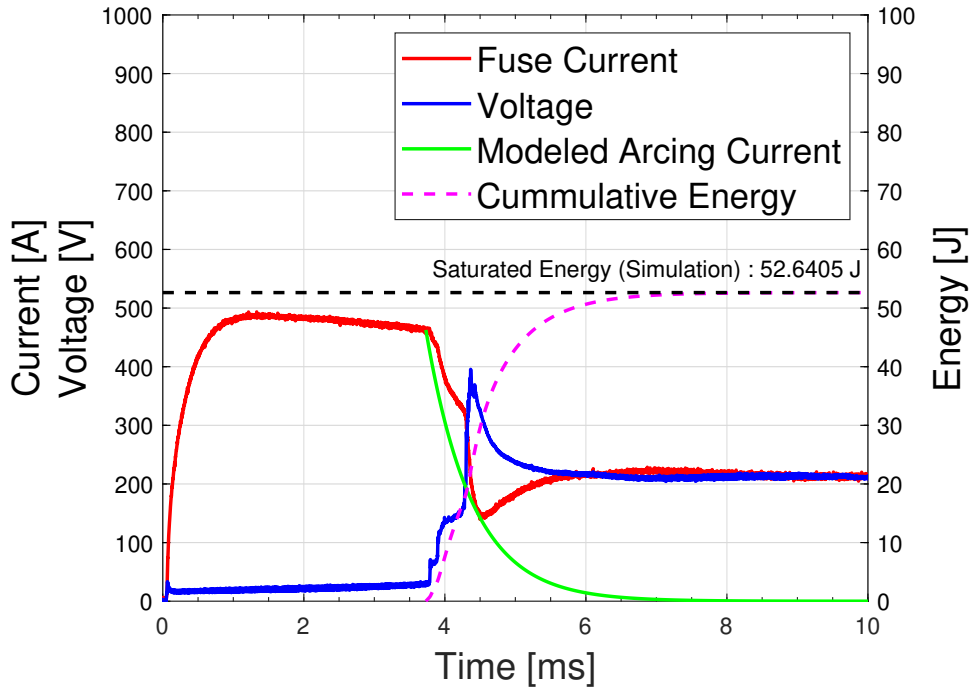

Figure 3.5: Arcing current model and minimum energy threshold of a glass fuse under explosive conditions

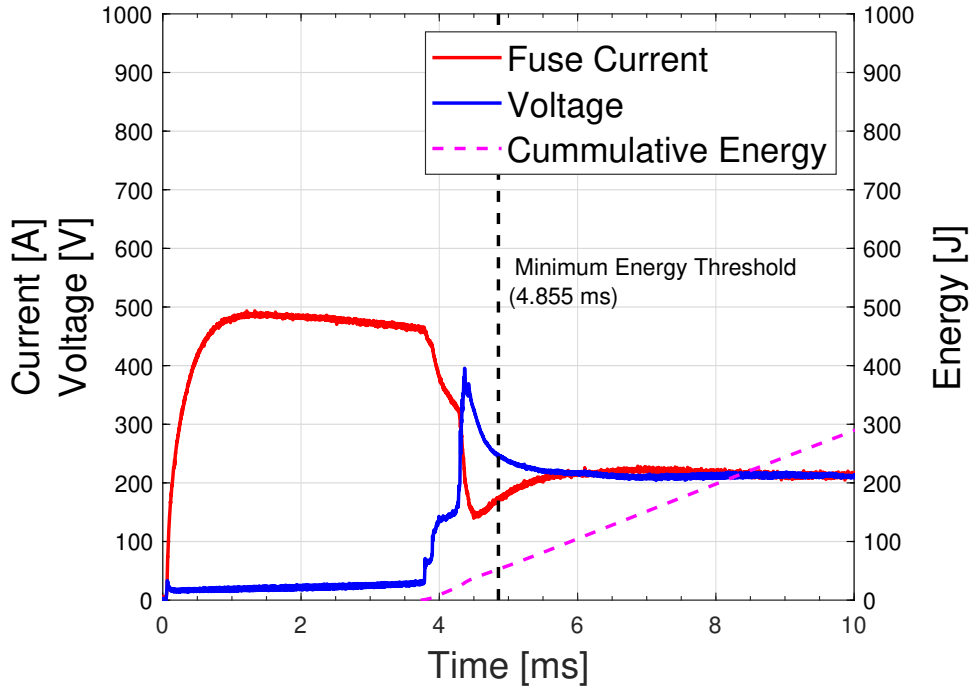

Figure 3.6: Estimated time to reach the minimum energy threshold in a glass fuse explosion test simulation

3.1.2 Maximum energy threshold calculation

To set the maximum energy threshold, Joule's law is applied using the previous experimental data:

$$\sum I[n] \cdot V[n] \cdot \Delta t \tag{3.1}$$

The observed current and voltage data are calculated with the sampling interval. Therefore, the maximum energy threshold is determined as 14.431 kJ using Equation 3.1 with current and voltage data up to 25 ms, just before the current surges again.

3.1.3 Workflow of the algorithm

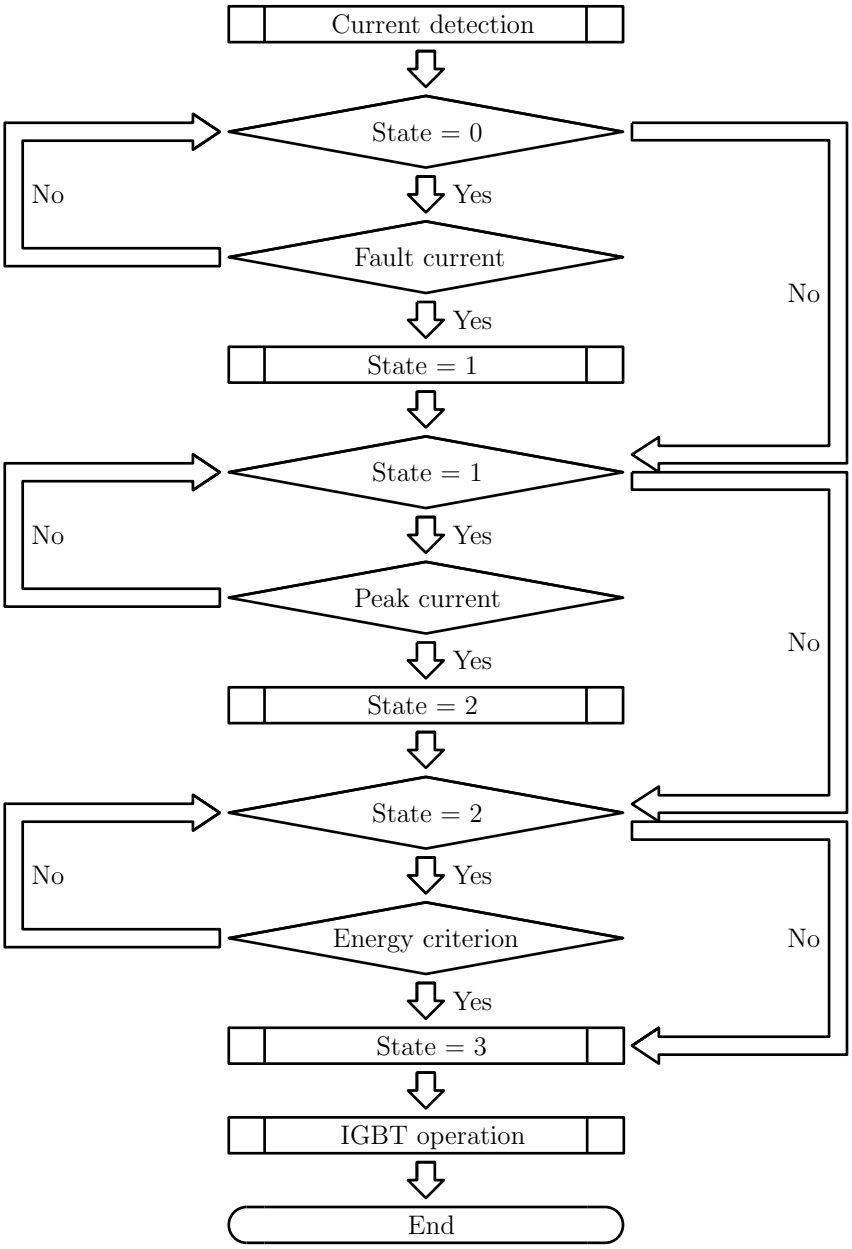

Figure 3.7: The workflow of the current-voltage-based commutation operation

The workflow of the proposed method is shown in Fig.3.7. State 0 and State 1 are identical to those in the current-based commutation method. The difference lies in State 2, where the fuse energy is calculated from the peak current and compared to the energy criterion. If the condition is met, a trigger signal is sent to the IGBT.

The pseudo-code for this workflow is provided below.

Algorithm 2 Process data for current-voltage-based commutation

```
Initialize State, Current, and other required variables.
if State = 0 then                                          ▷ State 0: Detect Fault
    if Current > FaultThreshold then
        StartTime ← CurrentTime
        PostSurgeData ← CollectData()
        State ← 1
    end if
end if
if State = 1 then                                          ▷ State 1: Detect Peak
    if DetectPeak(PostSurgeData) then
        PeakCurrent ← FindPeak(PostSurgeData)
        PeakTime ← CurrentTime
        State ← 2
    else
        PostSurgeData ← UpdateWindow(Current)
    end if
end if
if State = 2 then                                          ▷ State 2: Calculate Energy
    UpdateEnergy(Current, Voltage)
    if CommutationConditionMet() then
        TriggerIGBT()
        CommutationTime ← CurrentTime
        State ← 3
    end if
end if
if State = 3 then                                          ▷ State 3: Finalize Data
    if DataCollectionComplete() then
        WriteToSDCard(PostSurgeData, VoltageData, EnergyData)
        State ← 4
    end if
end if
```

3.2 Experimental validation

3.2.1 Experimental setup

The experimental circuit diagram is shown in Fig.3.8. Teensy 4.1 is applied as the MCU, and the MCU observes the current and voltage data in 50 kHz sampling frequency on the fuse branch with the calculation of the energy in real-time. It sends the operating signal to the IGBT when the accumulated energy is over the criterion. The R_i and C_i in the diagram is the RC circuit to protect the IGBT from the rapid increase in current and the high voltage, and 10 Ω and 642

μF, respectively. The experiment was carried out at 1.6 kV and 10 kA of the DC system. The applied energy criterion is 9 kJ, which is the medium value of the minimum (3.852 kJ) and maximum energy (14.431 kJ) threshold.

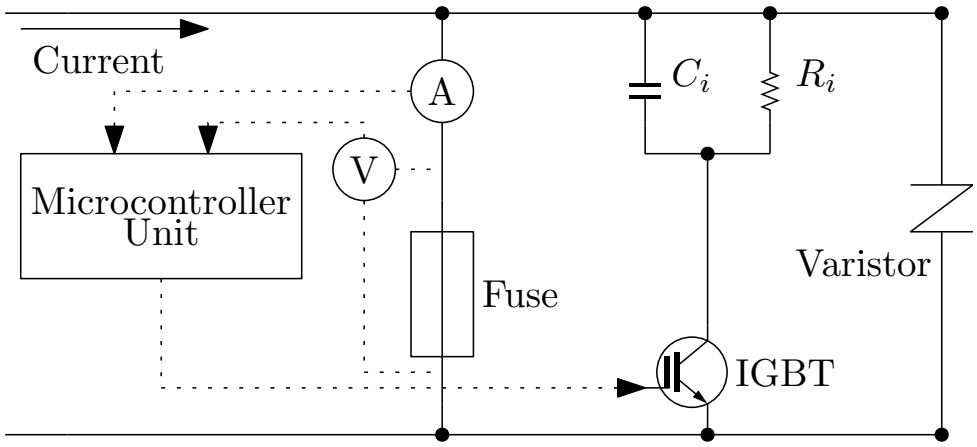

Figure 3.8: Circuit diagram for the current-voltage-based commutation validation experiment

Figure 3.9: Ceramic fuse tested in the experiment

The ceramic fuse used in the experiment is shown in Fig.3.9. The fuse size is approximately

5.5 times that of a 500 JPY coin, with a rated voltage of 1 kV and a rated current of 50 A.

The MCU configuration is presented in Fig.3.10. Five GPIO channels are used to handle the data. The ”V” cable detects the voltage across the fuse, while the ”C” cable measures the current. The ”PL” channel sends a trigger signal to the gate driver connected to the IGBT when the trigger condition is met. The ”MI” channel sends a signal to deactivate the IGBT by applying a negative voltage, preventing the operation caused by noise. Finally, the ”OS” channel allows monitoring of the MCU state through an oscilloscope. In addition, a bulb connected to the circuit changes color based on the state of the MCU, providing a visual indication.

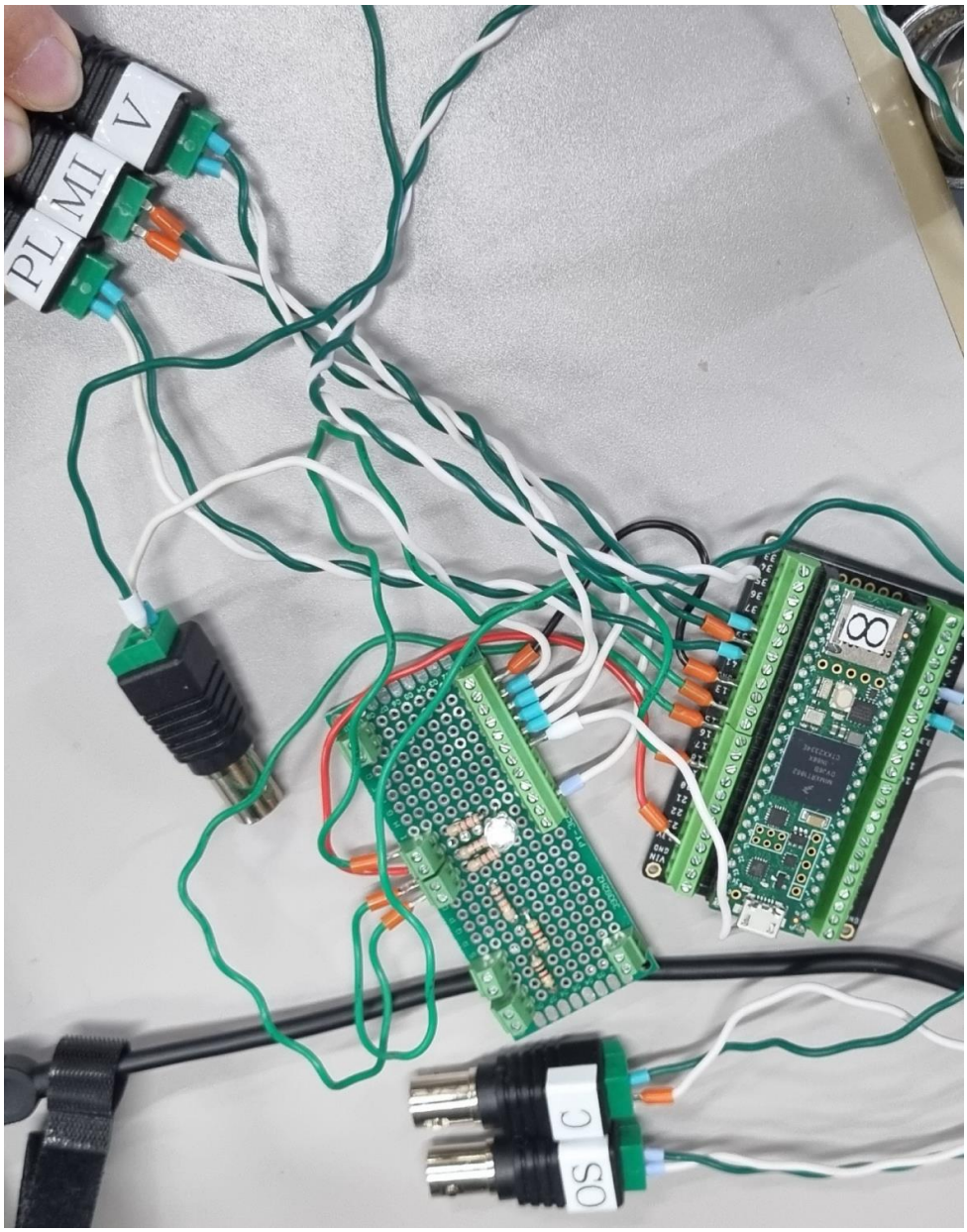

Figure 3.10: Microcontroller unit tested in the experiment

The following figure shows the entire experimental setup for the validation of the current-voltage-based commutation method. To prevent damage from potential explosions, the experimental circuit breaker, including components such as fuse, IGBT, and varistors, is placed in a room with durable walls. The MCU processes data from a current sensor with a magnification of 2000x and a voltage amplifier with a magnification of 1000x. This setup is necessary because the maximum voltage that Teensy 4.1 can handle is limited to 3.3 V. To detect up to 1.6 kV, the voltage amplifier is essential for the experiment. The same data is also observed through the oscilloscope, allowing the operation of the MCU to be monitored simultaneously.

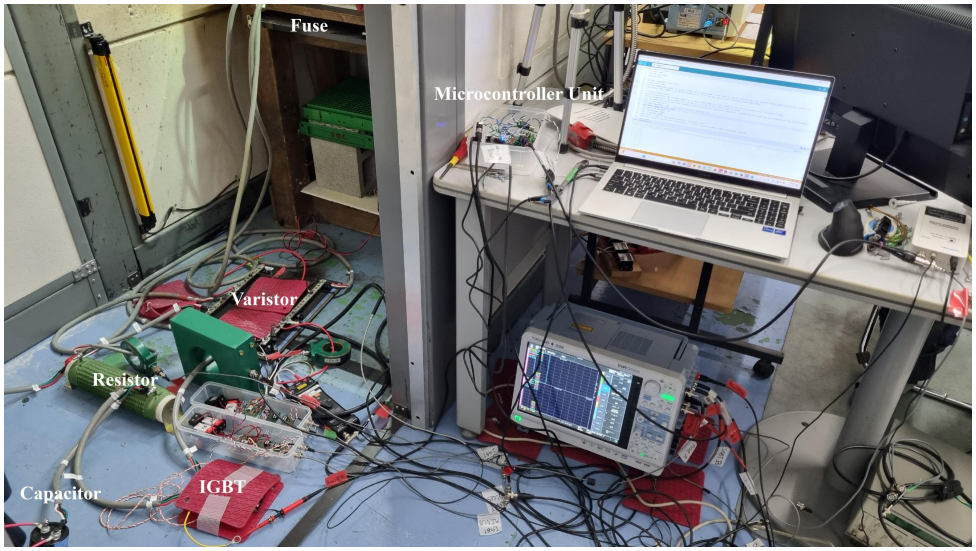

Figure 3.11: Actual experimental setup

3.2.2 Experimental results

Fig.3.12 shows the results. At $t = 0.521$ ms, the arcing phase begins after the maximum current. From this point on, the energy is calculated and continuously compared to the criterion. At $t = 24.330$ ms, the accumulated energy reaches the energy criterion, which triggers the IGBT.

In the oscilloscope data, the cumulative energy until commutation is recorded as 8.983 kJ, showing a 0.18% deviation from the energy criterion. This demonstrates that the MCU correctly estimates both current and voltage data simultaneously. The current path switches to the IGBT branch for 5 ms to isolate the fuse and prevent re-arcing. At $t = 29.552$ ms, the IGBT is turned off, completing the interruption.

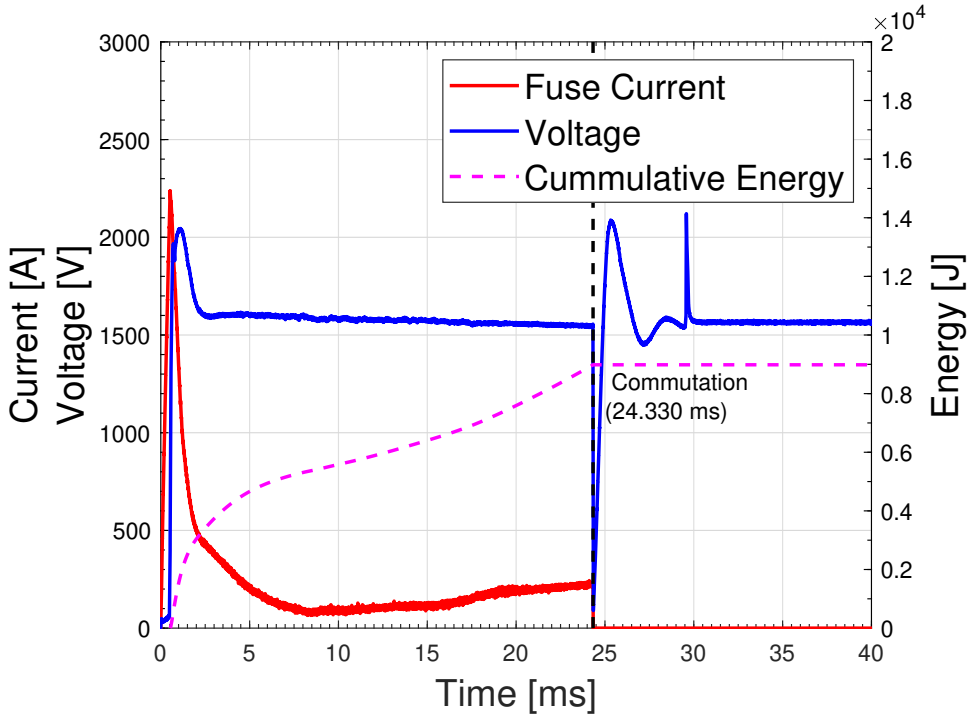

Figure 3.12: Current and voltage waveforms in current-voltage-based commutation experiment using a ceramic fuse under 1.6 kV and 10 kA

In this experiment, a single energy threshold was applied. The results confirm that the current and voltage data were obtained accurately and the energy was calculated precisely. Therefore, both the minimum and the maximum energy thresholds can be utilized in future applications. This approach prevents premature commutation, which could cause IGBT failure, and late commutation, which could result in fuse explosion.

3.3 Summary

In this chapter, the current-voltage-based commutation method was proposed. The energy threshold was used to estimate the fuse state in real-time.

The minimum energy threshold was simulated using the arcing current model with a single $\frac{1}{R_{\text{arc}}C_{\text{arc}}}$ value derived from previous experimental data. The maximum energy threshold was simulated on the basis of Joule's law, with the energy calculated using the data collected up to the resurge.

Based on this simulation, the energy criterion was established at 9 kJ and validated under

experimental conditions of 1.6 kV and 10 kA. The results demonstrated that the energy was accurately calculated in real-time and that the commutation was successfully started at t = 24.330 ms.

This approach addresses the limitations mentioned in Section 2.3.2. First, since the commutation method is based on energy, it provides a clearer explanation of the physical state of the fuse and the internal phenomena. Additionally, this method does not rely on the RLS algorithm to determine the commutation time, eliminating delays. The premature commutation error is resolved by the minimum energy threshold, which prevents commutation from occurring until the accumulated energy exceeds the threshold. This threshold also ensures that commutation does not occur when the fuse can independently interrupt the fault current.

Chapter 4

Conclusions and recommendations

4.1 Conclusions

This thesis focuses on fuse state estimation to determine the optimal commutation time for changing the current path in a fuse-semiconductor hybrid DC circuit breaker (CB) [1].

Although fuses have a simple structure, their operational characteristics are highly complex due to internal multiphysics phenomena [21]. To model these phenomena quantitatively, complex mathematical equations must be solved using various data, including thermal and electrical data [23]. This complexity makes it difficult to predict and control fuse performance in real-time.

The fuse-semiconductor hybrid DC CB simplifies this problem from a control engineering perspective, using the IGBT to regulate the fuse current. To actively determine commutation time, a current-based fuse state estimation method was proposed in previous research [22]. However, this method was validated under limited conditions using only a ceramic fuse. In this thesis, the versatility and applicability of the method were tested under various conditions.

The method was tested under three conditions, with two additional explosion experiments as follows:

- Fuse explosion experiments
  - Ceramic fuse explosion under 1.7 kV and 10 kA
  - Glass fuse explosion under 0.5 kV
- Validation of current-based commutation with a ceramic fuse

  - 1.7 kV and 10 kA
  - 0.95 kV and 10 kA

- Validation of current-based commutation with a glass fuse

The current-based method worked properly in these experiments. It was observed that the commutation condition was satisfied in two cases:

$$\frac{di(t)}{dt} = 0 \tag{4.1}$$

$$\frac{\frac{d^2i(t)}{dt^2}}{\frac{di(t)}{dt}} = \frac{\frac{di(t)}{dt}}{i(t)} \tag{4.2}$$

In the glass fuse waveform, commutation occurred generally when the current gradient changed from negative to positive. In the ceramic fuse waveform, commutation occurred when the first-order and second-order derivatives of the current data met a specific ratio.

However, several limitations of the current-based method were identified:

- Gap between physical phenomena and current data
- Delay in sending the signal to the IGBT
- Premature commutation error
- Commutation operation when fuse-only interruption is feasible

To address these limitations, this thesis proposes a current-voltage-based fuse state estimation method. The method uses an energy criterion to determine the commutation time, combining current and voltage data. Minimum and maximum energy thresholds are applied to set the criterion.

The minimum energy threshold was simulated using the arcing current model [25, 26] with a single $\frac{1}{R_{\text{arc}}C_{\text{arc}}}$ value derived from previous experimental data. The maximum energy threshold was simulated based on Joule's law, calculating energy from data collected up to the current resurge.

The simulation results set the energy criterion at 9 kJ, the midpoint between the simulated minimum and maximum thresholds. The method was tested under conditions of 1.6 kV and 10 kA, where commutation successfully triggered IGBT. While this experiment used a single

criterion, future applications could incorporate multiple thresholds, including minimum and maximum thresholds.

The proposed method and experimental results show that the limitations of the current-based method can be addressed. The current-voltage-based method observes energy, allowing for a clear estimation of the physical state of the fuse. In addition, the delay caused by the RLS algorithm is removed. The minimum energy threshold prevents premature commutation by ensuring that the trigger signal is sent only after the accumulated energy exceeds the threshold. This also ensures that commutation does not occur when the fuse can independently interrupt the fault current. These improvements enhance the reliability of commutation in the system.

4.2 Recommendations for future research directions

Although current-voltage-based fuse state estimation provides a reliable commutation method, several challenges remain.

Real-time minimum energy threshold calculation. In this study, the energy threshold is determined through simulations based on experimental data. However, the $\frac{1}{R_{\text{arc}}C_{\text{arc}}}$ parameter can be calculated in real-time. Therefore, implementing a real-time minimum threshold calculation should be further studied.

Application of parallel energy criteria. The energy criterion in this study is based on the average value of the minimum and maximum thresholds. To improve interruption speed and safety, it is suggested to validate the current-voltage-based commutation method using parallel criteria with both thresholds.

Fuse state estimation after commutation initiation. This research proposes a method to initiate commutation. Experimental results show that the plasma channel in the fuse disappears within 0.02 ms after the trigger signal is sent, reaching zero current. To further optimize the interruption process, it is recommended to study the IGBT operating time for effective fuse cooling and insulation based on fuse state estimation.

References

[1] S. Zen, Y. Inada, W. Ohnishi, Y. Fukai, N. Takayasu, M. Maeyama, and Y. Yamano, "Prototype current-limiting hybrid dc circuit breaker incorporating a fuse and a semiconductor device," *IEEE Transactions on Power Delivery*, vol. 36, no. 4, pp. 2231–2233, 2021.

[2] A. Mokhberdoran, A. Carvalho, H. Leite, and N. Silva, "A review on hvdc circuit breakers," in *3rd Renewable Power Generation Conference (RPG 2014)*, 2014, pp. 1–6.

[3] D. Jovcic, G. Tang, and H. Pang, "Adopting circuit breakers for high-voltage dc networks: Appropriating the vast advantages of dc transmission grids," *IEEE Power and Energy Magazine*, vol. 17, no. 3, pp. 82–93, 2019.

[4] X. Pei, O. Cwikowski, D. S. Vilchis-Rodriguez, M. Barnes, A. C. Smith, and R. Shuttleworth, "A review of technologies for mvdc circuit breakers," in *IECON 2016 - 42nd Annual Conference of the IEEE Industrial Electronics Society*, 2016, pp. 3799–3805.

[5] F. Mohammadi, K. Rouzbehi, M. Hajian, K. Niayesh, G. B. Gharehpetian, H. Saad, M. Hasan Ali, and V. K. Sood, "Hvdc circuit breakers: A comprehensive review," *IEEE Transactions on Power Electronics*, vol. 36, no. 12, pp. 13 726–13 739, 2021.

[6] W. Xiang, Y. Hua, J. Wen, M. Yao, and N. Li, "Research on fast solid state dc breaker based on a natural current zero-crossing point," *Journal of Modern Power Systems and Clean Energy*, vol. 2, no. 1, pp. 30–38, 2014.

[7] Y. Wang, W. Li, X. Wu, and X. Wu, "A novel bidirectional solid-state circuit breaker for dc microgrid," *IEEE Transactions on Industrial Electronics*, vol. 66, no. 7, pp. 5707–5714, 2019.

[8] Q. Guo, J. Zhang, and T. Chi, "Review of dc circuit breaker technology," in *2022 IEEE Sustainable Power and Energy Conference (iSPEC)*, 2022, pp. 1–5.

[9] J. Yin, X. Lang, and J. Duan, "Characteristic simulation of low voltage dc hybrid circuit breaker," in *2022 IEEE International Conference on High Voltage Engineering and Applications (ICHVE)*, 2022, pp. 1–4.

[10] Z. Liu, S. S. Mirhosseini, L. Liu, M. Popov, K. Ma, W. Hu, S. Jamali, P. Palensky, and Z. Chen, "A contribution to the development of high-voltage dc circuit breaker technologies: A review of new considerations," *IEEE Industrial Electronics Magazine*, vol. 16, no. 1, pp. 42–59, 2022.

[11] C. Meyer, M. Kowal, and R. De Doncker, "Circuit breaker concepts for future high-power dc-applications," in *Fourtieth IAS Annual Meeting. Conference Record of the 2005 Industry Applications Conference, 2005.*, vol. 2, 2005, pp. 860–866 Vol. 2.

[12] S. Sen, S. Mehraeen, and K. Smedley, "A bipolar hybrid circuit breaker for low-voltage dc circuits," in *2021 IEEE Energy Conversion Congress and Exposition (ECCE)*, 2021, pp. 1254–1260.

[13] M. Callavik, A. Blomberg, J. Häfner, and B. Jacobson, "The hybrid hvdc breaker," *ABB Grid Systems Technical Paper*, vol. 361, pp. 143–152, 2012.

[14] C. Ou, H. Yinming, and K. Yasuoka, "New configuration of contacts for increasing the threshold current of arc-free commutation in a dc hybrid switch," *IEEE Transactions on Components, Packaging and Manufacturing Technology*, vol. 10, no. 8, pp. 1320–1327, 2020.

[15] A. Hassanpoor, J. Häfner, and B. Jacobson, "Technical assessment of load commutation switch in hybrid hvdc breaker," in *2014 International Power Electronics Conference (IPEC-Hiroshima 2014 - ECCE ASIA)*, 2014, pp. 3667–3673.

[16] Y. Koyama, R. Morikawa, and T. Ishiguro, "Multi-line hybrid dc circuit breaker with low conduction loss and reduced semiconductor breaker," in *2019 21st European Conference on Power Electronics and Applications (EPE'19 ECCE Europe)*. IEEE, 2019, pp. P–1.

[17] S.-H. Park, J. W. Kim, and I.-D. Kim, "A new simple-structured thyristor hybrid dc circuit breaker," in *2021 24th International Conference on Electrical Machines and Systems (ICEMS)*, 2021, pp. 812–817.

[18] 稲. 優貴, 全. 俊豪, 大. 亘, 兒. 直人, 中. 裕介, 高. 康宏, 佐. 怜音, 宮. 優太, 塚. 幸佑, 山. 圭矢, and 山. 康, “ヒューズと半導体を併用した限流遮断器による低電圧システムの事故・負荷電流遮断,” **電気学会論文誌Ｄ（産業応用部門誌）**, vol. 144, no. 6, pp. 502–508, 2024.

[19] W. Ohnishi, Y. Inada, S. Zen, R. Sasaki, Y. Takada, Y. Miyaoka, K. Tsukamoto, and Y. Yamano, “Proof-of-concept of a fuse-semiconductor hybrid circuit breaker with a fast fuse exchanger,” *IEEE Transactions on Power Delivery*, 2022.

[20] S.-Y. Lee, Y.-K. Son, H.-J. Cho, S.-K. Sul, S.-H. Kim, N.-S. Kang, and W.-J. Park, “Simplified thermal model of semiconductor fuse for dc distribution system,” in *2019 10th International Conference on Power Electronics and ECCE Asia (ICPE 2019 - ECCE Asia)*, 2019, pp. 2641–2646.

[21] M. Horn, L. Brabetz, and M. Ayeb, “Data-driven modeling and simulation of thermal fuses,” in *2018 IEEE International Conference on Electrical Systems for Aircraft, Railway, Ship Propulsion and Road Vehicles & International Transportation Electrification Conference (ESARS-ITEC)*, 2018, pp. 1–7.

[22] Y. Liu, R. Sasaki, W. Ohnishi, K. Yamada, T. Kobayashi, Y. Inada, Y. Yamano, and S. Zen, “Verification of fuse-semiconductor commutation based on online estimation of fuse current-limiting status,” in *IEE Japan* **全国大会**, 2024, pp. 36–37.

[23] A. Plesca, “Numerical analysis of thermal behaviour of dc fuse,” *Energies*, vol. 13, no. 14, 2020. [Online]. Available: https://www.mdpi.com/1996-1073/13/14/3736

[24] S. Kim, T. Shin, S. Jeong, H. Kang, K. Son, S. Park, H. Kim, J. Choi, M. Kim, H. Kim, and J. Kim, “Modeling and verification of a high voltage fuse for high reliability and safety in electric vehicle,” in *2020 IEEE International Symposium on Electromagnetic Compatibility & Signal/Power Integrity (EMCSI)*, 2020, pp. 287–292.

[25] T. Tanaka, H. Kawaguchi, T. Terao, T. Babasaki, and M. Yamasaki, “Modeling of fuses for dc power supply systems including arcing time analysis,” in *INTELEC 07 - 29th International Telecommunications Energy Conference*, 2007, pp. 135–141.

[26] D. Li and L. Qi, “Energy based fuse modeling and simulation,” in *2013 IEEE Electric Ship Technologies Symposium (ESTS)*, 2013, pp. 487–492.

[27] H. Sang-Ok, “Empirical modeling on the breaking characteristics of power current limited fuse,” *The Transactions of the Korean Institute of Electrical Engineers C*, vol. 54, no. 9, pp. 391–396, 2005.

[28] A. J. Allen, S. Chopra, S. Santoso, and T. A. Short, “Unique waveform characteristics of current limiting fuse operations,” in *IEEE PES General Meeting*, 2010, pp. 1–6.

[29] A. Bahman, S. Jensen, and F. Iannuzzo, “Failure mechanism analysis of fuses subjected to manufacturing and operational thermal stresses,” *Microelectronics Reliability*, vol. 88-90, pp. 304–308, 2018, 29th European Symposium on Reliability of Electron Devices, Failure Physics and Analysis (ESREF 2018). [Online]. Available: https://www.sciencedirect.com/science/article/pii/S0026271418305298

[30] H. Ji, J. Kim, J. Song, Y. Choi, C. Park, N. Park, and G. Kil, “An experimental study on melting characteristics of low-voltage miniature cartridge fuse,” *Journal of the Korean Society of Safety*, vol. 28, no. 5, pp. 15–20, 2013.

[31] S. Eio and N. Shammas, “Igbt tail current reduction by current injection technique,” in *2008 43rd International Universities Power Engineering Conference*, 2008, pp. 1–4.

Publication

Domestic conference (no peer-reviewed)

1. S. Shin, R. Sasaki, Y. Nakano, N. Kodama, S. Zen, Y. Yamano, Y. Inada, and W. Ohnishi: “Experimental Validation of Optimized Sequence Control for Fuse Current Under Diverse Conditions,” IEE Japan 開閉保護研究会 [編] 2024 (1-7), pp.33-37, (2024)

2. S. Shin, R. Sasaki, W. Ohnishi, Y. Nakano, N. Kodama, S. Zen, Y. Yamano, and Y. Inada: “Real-Time Energy Calculation of Fuse for Commutation Control in Fuse-Semiconductor Hybrid DC Circuit Breaker,” IEE Japan 全国大会 (2025 Scheduled)

International conference (peer-reviewed)

1. S. Shin, R. Sasaki, Y. Nakano, N. Kodama, S. Zen, Y. Yamano, Y. Inada, and W. Ohnishi: “Optimized sequence control of a fuse-semiconductor hybrid circuit breaker through real-time fuse state estimation,” Conf. on 2024 IEEE Industrial Electronics Society (IECON), (2024)

Awards

1. Student and Young Professionals (SYP) Paper Assistance and Travel Award, Conf. on 2024 IEEE Industrial Electronics Society (IECON), (2024)